airestech

400 APPLEWOOD CRESCENT UNIT 100
VAUGHAN, ONTARIO, L4K 0C3, CANADA
1 (855) 725-2034 | WWW.AIRESTECH.COM

American Aires Inc.
Research and Development department

REPORT

R&D: Calculation of the strength and intensity of the electromagnetic field in the interaction of electromagnetic radiation at a frequency of 2.4 GHz (WiFi) with an Aires C28S resonator (microprocessor), which is used in the Aires Defender Pro (2018 model)

Project manager:
I. Serov

Responsible researcher:
K. Korshunov

Researchers:
I. Soltovskaya
T. Shamko

Consultants:
Prof. Dr. of Technical Sciences A. Kopyltsov
Prof. Department of Physics Dr. A. Jukna

2018

TABLE OF CONTENTS

Introduction.
1. Physical model.
2. Mathematical model.
3. Calculation parameters.
4. Algorithm for the calculation.
5. Results and discussion.

Conclusion.
Appendix 1. Topology of the resonator (microprocessor) Aires C28S.
Appendix 2. Hardware and software.
Appendix 3. Animation.

INTRODUCTION

To simulate the processes occurring in the interaction of Aires resonators (microprocessors), which are manufactured using Micro-Electro-Mechanical Systems (MEMS) technology, with electromagnetic radiation, physical models of such interaction, as well as algorithms and computer programs based on them, were developed.

This software development was necessary, because the various software packages available on the market generally consider interactions in the context of classical physics. However, a number of studies have shown that the processes taking place in this case can only be explained by accounting for the counter wave interaction on the surface of the resonator and the numerous derivative resonances that result from these processes. Existing packages do not take these factors into consideration.

The following experiment with the Aires resonator (microprocessor) showed the possibility of using it in a new class of devices used in medicine, energy conservation, and protecting humans from man-made electromagnetic radiation.

This report discusses the interaction of electromagnetic radiation at a frequency of 2.4 GHz with an Aires resonator (microprocessor) with the C28S topology (Appendix 1), which is used in the Aires Defender Pro (2018 model). The calculations were made on hardware using software (Appendix 2).

In order to most closely approximate specific technical problems: the design of the simulated element, the range of electromagnetic radiation corresponding to the frequency of a WiFi router (2.4 GHz) and other modern mobile communication devices, the following physical model was considered in the simulation.

1. PHYSICAL MODEL

Aires resonators (microprocessors) are self-affine circular diffraction gratings with a fractalization factor of 2 and a number of fractalization axes corresponding to the number of the topological circuit (from 8 to 32).

Characteristics of the Aires C28S microprocessor

- Number of fractalization axes: 28
- 4 levels of fractalization:

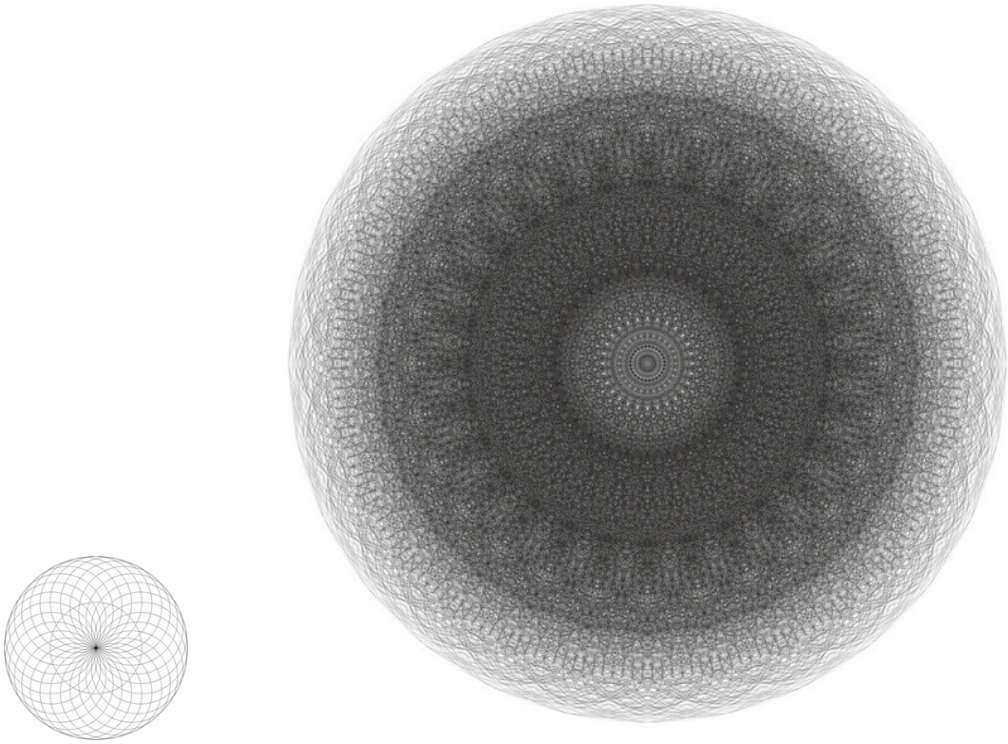

Basic module, D = 4.6 mm

General view of the circuit, D = 18.4 mm

Fig. 1. Topology of the Aires C28S resonator (microprocessor), which is a flat cut through the center of the self-affine hypersphere

- Number of rings (slit resonators): 707281
- Slit parameters (width / height): 0.4 μm / 0.8 μm.

The axes are arranged in pairs, strictly along the diameters of the circuit, thereby forming counter-resonance interaction corresponding to formula (1), which describes the principle of equilibrium of a hypercomplex system of interactions, based on the maximally deep space-time amplitude-frequency harmonization of the wave fronts, which correlates with the Schrödinger superposition principle, which expresses the emerging wave superposition as the

vector sum of all the relationships between the elements participating in the process. This is possible only as a result of the interaction of absolutely adequate counter functions, i.e. the elements of the system participating in the process must be coordinated among themselves in terms of amplitudes, frequencies, phases (system focal point), and the interaction diagram. This process makes it possible to locally accumulate and use the highest potential.

When presenting the base unit of the system as B_0 (x_1, x_2, ..., x_n), and the functions of the fractal mapping (for example, scaling and shifting) through $F(B_0)$, the iterative process of the formation of the fractal structure, which reflects the hierarchical principle of the structural organization of the counter interaction system, can generally be described as:

$$F_k(B_0) = \sum_{i=1}^{k-1} F_i(B_0)$$

.

The level of contradictions within any arbitrarily taken hypercomplex system, if obtaining a functionally active and maximally stable design is required, should tend to zero, defining the principle of universal multi-level coordination (coherence). The statement applies to both a three-dimensional "X, Y, Z" system, and to a self-affine hyperspherical form whose number of structural components of different dimensionality tends to infinity.

For the case of the reciprocal vector interaction, the equation can be written as:

$$X^n + Y^n + Z^n + \ldots + N^n \rightarrow 0$$

This expression implies the simultaneous solution of all equations comprising the given spatial hypercomplex. The number of these equations is equal to the number of interactions that define the process under consideration.

In the case of interaction of system-wide hyper-objects of different fractal dimensions with respect to a common "zero" center (a phase transition to the next quantum fractalization zone), the equation takes the form:

$$\sum_{k=1}^{n} X^k + \sum_{k=1}^{n} Y^k + \sum_{k=1}^{n} Z^k + \cdots + \sum_{k=1}^{n} N^k \rightarrow 0 \qquad (1),$$

where 0 is the focal point (center point) of the circuit, which is a singularity zone where the potential density tends to infinity and its amplitude approaches zero.

The resonators' topological circuits have the properties of the self-affine analogs of fractal antennas. A fractal antenna is an antenna whose active part has the form of a self-similar curve or any other figure similarly divided or consisting of similar segments.

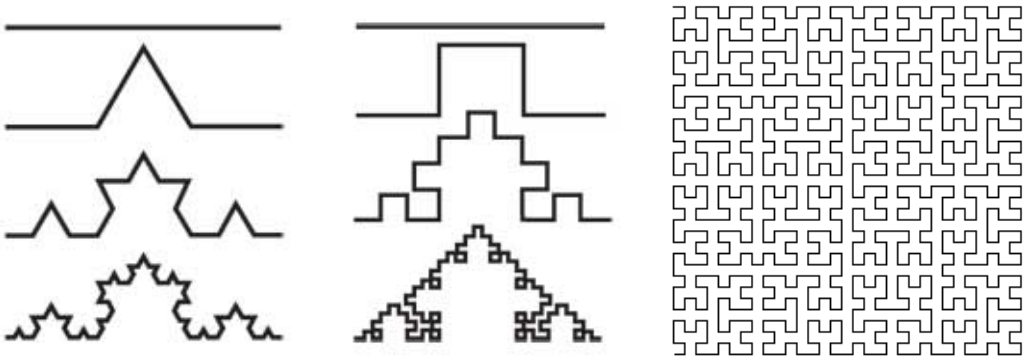

Fig. 2. Emitters based on Koch and Peano fractals

It should be noted that any system that adheres to the same principle for forming constituent elements, for example, the Fibonacci series, will also be a fractal object, i.e. will have the properties of self-similarity and scale invariance.

Typically, almost all biological objects widely represented in nature tend to form corresponding fractal structures by multiplying the self-similar structural elements (Fig. 3) that form their basis.

Fig. 3. Fractals in nature

This is due to the need to interact with the widest possible range of electromagnetic radiation frequencies in the environment for the purpose of accumulating the energy-information potential necessary for the vitality of any biological organism (metabolism and homeostasis processes) and adequately systematized reversal of genetic programs in the process of its synthesis. An analogous process associated with the presence of the required level of harmonized energy potential is also observed in inanimate nature in the formation of the structures of any crystal lattices (Figures 4, 5).

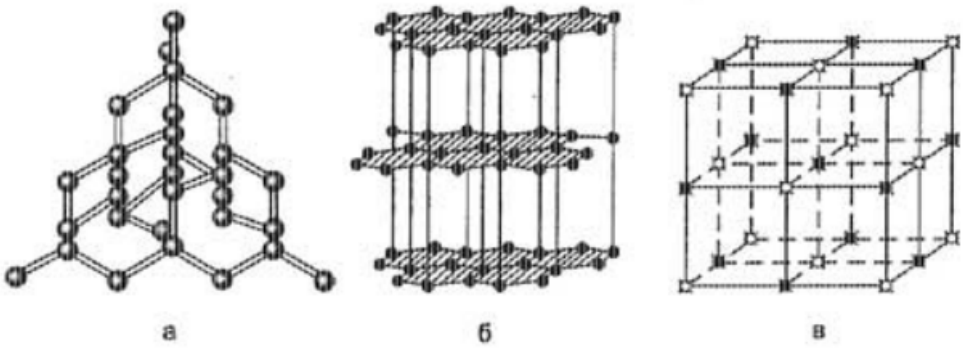

Fig. 4. Crystal lattices: a) diamond, b) graphite, c) rock salt

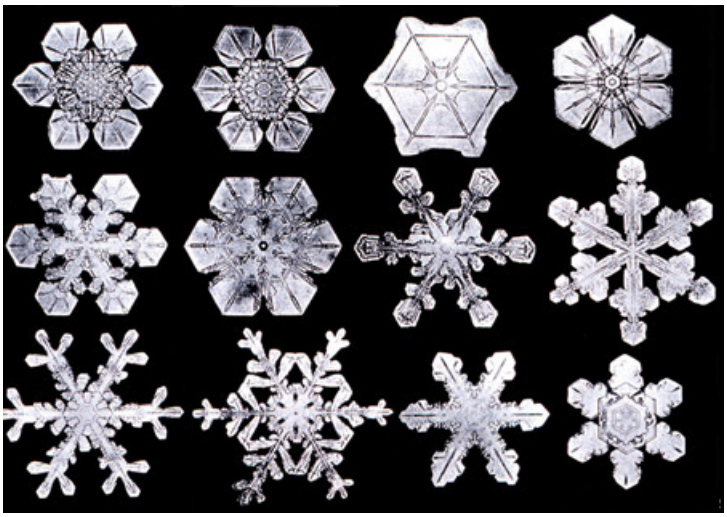

Fig. 5. Photographs of ice crystals

The specific properties of the Aires resonator (microprocessor) as a fractal ring diffraction grating are broadband interaction with external electromagnetic radiation and a high degree of signal amplification due to the summation of currents and the resulting iterative resonance effect as an integral superposition of subresonant processes. Thus, the resonator may be considered an analog of a fractal antenna.

The total length of the rings forming the resonator's self-affine matrix as a conductor is composed of the sums of circumferences that form its topological circuit and determines the lower boundary of the frequency range of the resonator's interaction with incident electromagnetic radiation (Table 1).

Table 1.

Microprocessor No.	**C28S**
Ring diameter	2300 μm
Number of rings	707281
Length of the conductor (antenna)	164.41 m
Lower threshold of interaction frequency	1.82 MHz

Because the Gabor-Denisyuk hologram theory says that any wave superposition has the same properties as the regular system that generated it, we can consider the wave superposition (hologram) arising from the material regular circuit (Fig. 1) as the first derivative, which has the corresponding properties of the base grating that gave rise to it. In turn, the analogous transform of external radiation, which arises based on the first derivative of the external radiation, can be regarded as the second derivative. Finally, the transformed second derivative of the wave processes' interaction with each other can be considered the third derivative, which always represents a deepened interference, i.e. including the interaction of waves, half-waves, and quarter waves, thus forming a three-level system of resonant relationships. In the end, the result of this process as the fourth derivative is the process of harmonizing the different types of external radiation through the structure of the second derivative giving rise to this process (superposition from a regular fractal base), which in this case acts as a universal filter initiating a direct and inverse Fourier transform. Thus, there is a differentiation of the initial wave flow (2.4 GHz) into eigen harmonics with the subsequent formation of a matrix of electromagnetic superpositions that is spatially-temporally harmonized with respect to the amplitudes and frequencies.

The Aires resonator (microprocessor) is a type-n monocrystalline silicon substrate with a crystallographic plane of 100 (Miller index), with dimensions of 19.4 mm x 19.4 mm and a thickness of 0.5 mm, whose surface has a fractal system of annular slits with a rectangular cross section with a width of 0.4 μm and depth 0.8 μm, forming a regular self-affine structure that obeys the laws of self-similarity and scale invariance (Appendix 1).

The incident radiation's interaction with the silicon substrate produces polarization and a surface wave.

According to modern scientific knowledge, everything is electromagnetic in nature. A material's crystal lattice is a certain ordered, periodic field structure. Erwin Schrödinger, an Austrian Nobel laureate and one of the founders of quantum physics, was the first to express this idea. In turn, any material structure creates a periodic electromagnetic field (superposition) and is maintained by this same field. Moreover, the perfect structures initiate a maximally coherent response that is strictly systematized in terms of amplitudes, frequencies, phases, and the interaction diagram.

Hence we can draw the following conclusion: since the silicon substrate has an appropriate crystal lattice whose domains can be regarded as a regular system of conductors representing a fractal complex, the total length of such domains will determine the wavelength and the frequency range of the object's response to external electromagnetic radiation. Of course, this phenomenon requires additional research.

When the resonator interacts with the radiation incident on its surface, a surface wave appears and is reflected from the surface with absorption in the slits, which leads to a redistribution of the characteristics of the electromagnetic field. The resonator's slit structure can be considered as a regular topology of the surface of a self-affine silicon wafer (substrate).

Both the distribution of the electric field strength above the resonator surface and the distribution of the field's energy flux density (intensity) were modeled.

2. MATHEMATICAL MODEL

In the modeling, it is assumed that the charge carriers are concentrated in the slits. Thus, the potential density and, accordingly, the calculated intensity within the slit will depend on its geometry. In our case, since the slit width b = 0.4 μm and the slit depth glu = 0.8 μm, when an electromagnetic wave passes through the resonator surface during interaction with a slit, we consider two variants of wave propagation: movement over the slit (path l_1) and motion along the slit (path l_2):

$$l_1 = b = 0.4 \text{ (μm)},$$

$$l_2 = b\ 2 * glu = 5b = 5 * 0.4 = 2.0 \text{ (μm)}.$$

Thus, the path difference is:

$$\Delta l = l_2 - l_1 = 5b - b = 4b = 4 * 0.4 = 1.6 \text{ (μm)}.$$

If the initial strength on the surface of the resonator has a gain of 1, then it can reach a maximum of 4 in the slits. To calculate the strength, a gain coefficient K_l = 2 ÷ 4 depending on the density of the resonator's topological circuit, i.e. in low density areas of the circuit K_l= 2, in high density zones K_l= 4.

$$E_0` = E_0 * K_l ,$$

where E_0 is the initial (background) electric field strength,
$E_0`$ is the electric field strength, including the gain.

To describe the current calculation model, it is assumed that the source radiation falls on the AIRES resonator (microprocessor) uniformly from all sides. Thus, we have a radiation source in the form of a hemisphere with radius R, which is significantly greater than the diameter of the resonator.

The radiation is distributed along the DCA trajectory (Fig. 6). Point D is on the sphere with radius R. Point C is on the resonator wafer. Point A is on the receiver (the space above the resonator wafer), and the strength of electric field E is determined at this point. Point C has 2 possible locations – in the slit and on the surface of the resonator. If point C is on the surface, then the incident radiation at point C is reflected (the angle of incidence is equal to the angle of reflection). If point C is in the slit, then the incident radiation at point is absorbed.

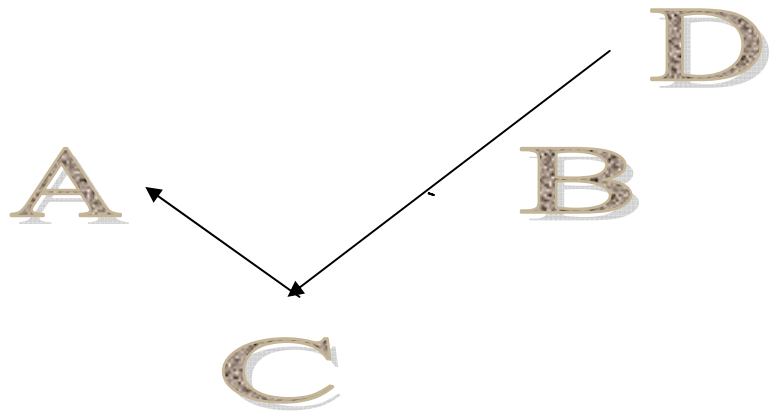

Fig. 6. Trajectory of the incident radiation DCA.

The smooth surface of the resonator is broken into square cells with side h and point C successively (in a cycle) traverses every node in this two-dimensional grating. The receiver is the three-dimensional space around the resonator, divided into cubic cells with side h and point A successively (in a cycle) traverses every node in this three-dimensional grating. At each time t , the coordinates of points A (on the receiver) and C (on the resonator) are assumed to be known.

We assume that we know the intensity of the incident radiation E_0 and the frequency of the radiation ω at point D (radiation source).

We need to find: the strength of electric field E at point A (receiver).

If the coordinates of points A (x_A, y_A, z_A) and C (x_C, y_C, z_C) are known, then the coordinates of point B (x_B, y_B, z_B) can be determined using the following formulas:

$$x_B=2\,x_C-x_A$$
$$y_B=2\,y_C-y_A$$
$$z_B=z_A$$

Point B is symmetric to point A in the DCA plane relative to the normal to the resonator's surface at point C.

Equation for the line segment BC:

$$\frac{x-x_C}{x_B-x_C}=\frac{y-y_C}{y_B-y_C}=\frac{z-z_C}{z_B-z_C}$$

Equation for the line segment AC:

$$\frac{x-x_C}{x_A-x_C}=\frac{y-y_C}{y_A-y_C}=\frac{z-z_C}{z_A-z_C}$$

Distance between points A and C:

$$L1=\sqrt{(x_A-x_C)^2+(y_A-y_C)^2+(z_A-z_C)^2}$$

Coordinates of vector CA:

$$x_{CA}=x_A-x_C$$
$$y_{CA}=y_A-y_C$$
$$z_{CA}=z_A-z_C$$

Direction cosines of vector CA

$$cos(CA_x)=x_{CA}/L1$$
$$cos(CA_y)=y_{CA}/L1$$
$$cos(CA_z)=z_{CA}/L1$$

Equation for sphere with radius R with center at (x_0, y_0, z_0) (coordinates of the center of the resonator):

$$(x-x_0)^2+(y-y_0)^2+(z-z_0)^2=R^2$$

The coordinates of point D (x_D, y_D, z_D), the intersection of line segment BC and the sphere with radius R, are determined from the following system of equations:

$$\frac{x-x_C}{x_B-x_C}=\frac{y-y_C}{y_B-y_C}=\frac{z-z_C}{z_B-z_C}$$
$$(x-x_0)^2+(y-y_0)^2+(z-z_0)^2=R^2$$

Distance between points C and D:

$$L2=\sqrt{(x_D-x_C)^2+(y_D-y_C)^2+(z_D-z_C)^2}$$

The length of the DCA is equal

$$L=L1+L2$$

The sphere with radius R radiates a monochromatic wave with frequency ω and wavelength $\lambda=\frac{2\pi V_C}{\omega}$ and speed of light V_C.

At time t, the strength of the electric field (created by the DCA beam) at point A is equal to

$$E=E_0\cos(\omega(t-\frac{L}{V_C}))$$

where E_0 is strength of the incident radiation.

The projections of E (created by beam DCA) on axes X, Y and Z at point A at time t are equal to:

$$E_x=E\ cos(CA_x),\ E_y=E\ cos(CA_y),\ E_z=E\ cos(CA_z)$$

The projections of E (created by the resonator) on axes X, Y and Z at point A at time t are equal to the amount of the projections of E (created by

beams DCA), where point C passes each node of the square cells into which the resonator is divided:

$$E_x^{resonator} = \sum_{resonator} E_x, \quad E_y^{resonator} = \sum_{resonator} E_y, \quad E_z^{resonator} = \sum_{resonator} E_z.$$

The strength of electric field E (created by the resonator) at point A at time t is equal to

$$E_A^{resonator} = \sqrt{(E_x^{resonator})^2 + (E_y^{resonator})^2 + (E_z^{resonator})^2}$$

Given time change Δt, we can calculate the strength of electric field E at any point of the receiver at any point in time.

The results are output as 4-dimensional matrices (the coordinates of the point at which E is calculated, and the time):

$$E_A^{resonator}, \quad E_x^{resonator}, \quad E_y^{resonator}, \quad E_z^{resonator}.$$

To following formula is used to account for diffraction:

$$\frac{I_\beta}{I_0} = \frac{\sin^2(\frac{\pi b}{\lambda}\sin\beta)}{(\frac{\pi b}{\lambda}\sin\beta)^2},$$

where I_β is the intensity of waves propagating at an angle β, I_0 is the intensity of waves propagating at an angle β=0, b is the width of the slit, β is the angle, λ is the wavelength. Because the intensity of the wave is proportional to the square of the amplitude,

$$\frac{I_\beta}{I_0} = \frac{E_\beta{}^2}{E_0{}^2} = \frac{\sin^2(\frac{\pi b}{\lambda}\sin\beta)}{(\frac{\pi b}{\lambda}\sin\beta)^2},$$

$$E_\beta = E_0 \frac{\sin\ (\frac{\pi b}{\lambda}\sin\beta)}{\frac{\pi b}{\lambda}\sin\beta}.$$

Thus, in the end in general we have a vector E:

$$E = E_{otr} + E_{difr},$$

where E_{otr} is due to reflection, E_{difr} is due to diffraction (in the case of narrow slits).

3. CALCULATION PARAMETERS

1. The topological circuit of the Aires resonator (microprocessor) is considered a self-affine annular diffraction grating made in the form of slits with the following dimensions: $0.4 * 10^{-6}$m x $0.8 * 10^{-6}$m (0.4 μm x 0.8 μm, width and depth).
2. Resonator dimensions: $19.4 * 10^{-3}$m x $19.4 * 10^{-3}$m x $0.5 * 10^{-3}$m (19.4mm x 19.4mm x 0.5mm).
3. The resonator interacts with the radiation emitting from the WiFi-source (router) in the form of a large-diameter hemisphere (the diameter of a sphere larger than the wafer dimensions). The distance from the source to the resonator is 10 m.
4. The surface of the resonator reflects radiation (absorption is not considered), but the slits absorb (reflection in the slits is not considered).
5. Parameters of the incident radiation:
   - strength E_0= 10 V/m; (manufacturer data)
   - frequency ω = 2.4 GHz.
   - field strength $E \sim \omega^2 = (2.4\ \text{GHz})^2 \sim 5.76$ (W/m);
   - flux density $I \sim \omega^4 = (2.4\ \text{GHz})^4 \sim 0.33$ (W / m^2).
6. The resonator surface is divided into square cells in increments of $h = 22.5 * 10^{-6}$m (22.5 μm).
7. The resulting radiation is calculated in the space above the resonator, divided into cubic cells with an increment of h.
8. The electromagnetic radiation interacts with the resonator for t = 1 s.
9. The time spent on the calculations is 120 machine-hours.

4. ALGORITHM FOR THE CALCULATION

The algorithm for the calculation generally looks like this:

1. An Aires resonator (microprocessor) with the C28S topology (Appendix 1) is located in the center of the cubic matrix, i.e. the dimension of the matrix is the same along all axes X, Y, and Z. Calculations are performed for the upper half of the cubic matrix. Then the results are mirrored for the lower half. As a result, we obtain a matrix that is symmetric with respect to the plane on which the resonator is placed, and a cubic matrix of the results of the initial strength calculation *E* – "Derivative 1».

2. To record the spatial representation of the relevant processes, in this stage we take the matrix and add copies of it that have been rotated 45° about the X, Y, and Z axes and sum up the results. In the resulting cubic matrix, we identify the general sphere-shaped area that contains all summed elements, and we call it "Derivative 2".

3. Next we project "Derivative 2", with center at the origin (the center of the resonator) and radius R1, by a distance equal to radius R1 in 198 directions and sum the results (199 spheres). We end up with a cubic matrix that contains a sphere with radius $R2=2*R1$, which we call "Derivative 3".

5. RESULTS AND DISCUSSION

For the most complete and adequate understanding of the processes, the model was initially considered and calculations of the incident electromagnetic radiation's interaction with the resonator surface and the diffraction response that was induced on it. The resonator is a ring with a radius of 1150 μm with given slit parameters (depth - 0.4 μm, width - 0.8 μm), which is the basic structural element of the topology of the Aires C28S resonator (microprocessor). The results are shown in Fig. 7.

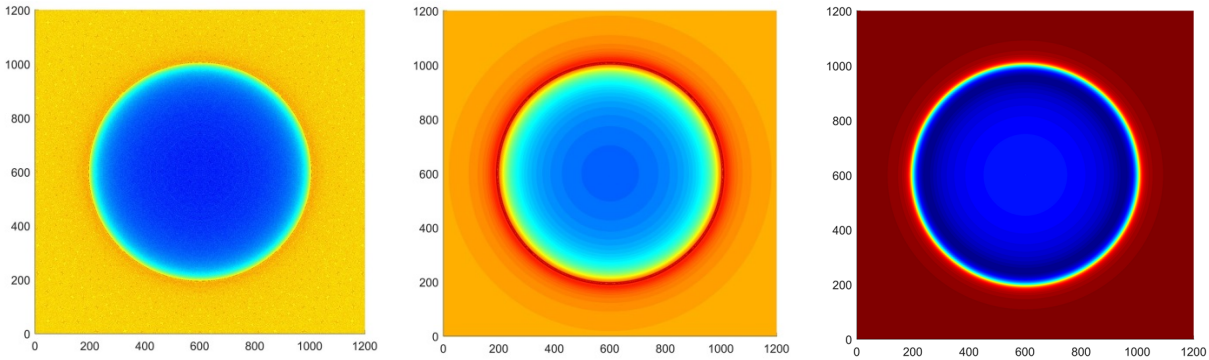

a) *b)* *c)*

*Fig. 7. Diffraction response on the 1s ring: a) ν = 2.4 * 10^{21}Hz (gamma radiation), b) ν = 5.5 * 10^{15}Hz (green spectrum of the Sun), c) ν = 2.4 * 10^{9}Hz (Wi-Fi radiation)*

As can be seen from Fig. 7, the interaction produces an annular spectrogram. In the case of gamma radiation, a fractal structure is formed inside the ring as a result of integral interaction of waves (superposition), and outside - analogous to natural objects (Fig. 8).

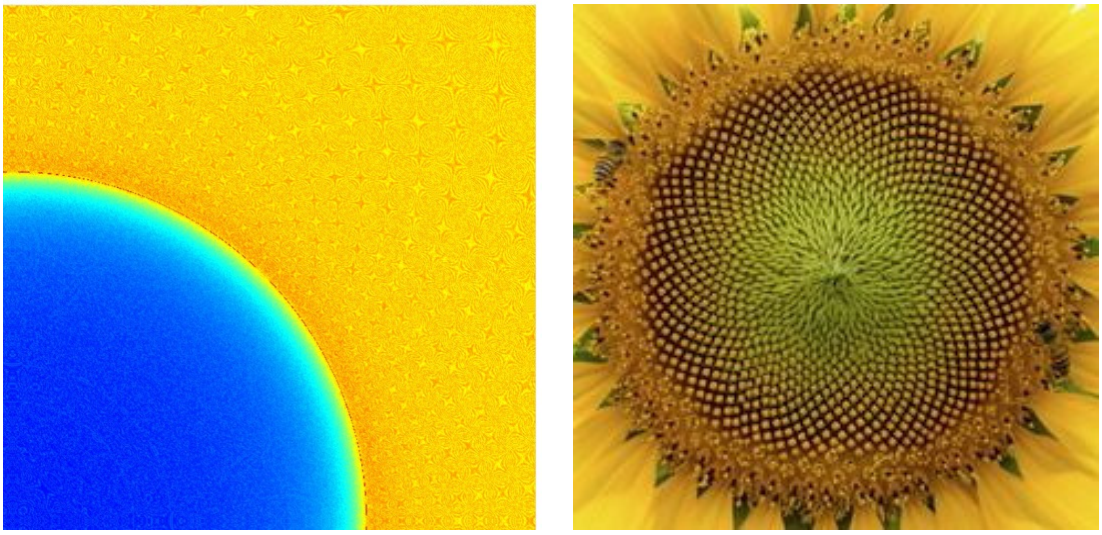

Fig. 8. Fragment of the image from Fig. 7a) and a photo of a sunflower

The ring shape has a specific feature in that, since its surface is curved and has a focal point located at the center of the ring, an impulse striking the interior begins to move along a trajectory that intersects this point and, upon reaching the opposite surface of the ring, is reflected and returned, again intersecting the focal point. Thus, the appearance of an absolutely adequate counter function begins resonant self-generation of the potential.

In turn, electrons begin to move along the annular slit, which provokes the formation of an opposing wave stream, and when their phases coincide, a standing wave is formed.

The 1st step of the calculation is "Derivative 1".

In accordance with the algorithm, the calculations were performed in 3 stages. The result of the first stage is a matrix of the strength of the electric field *E* over the resonator.

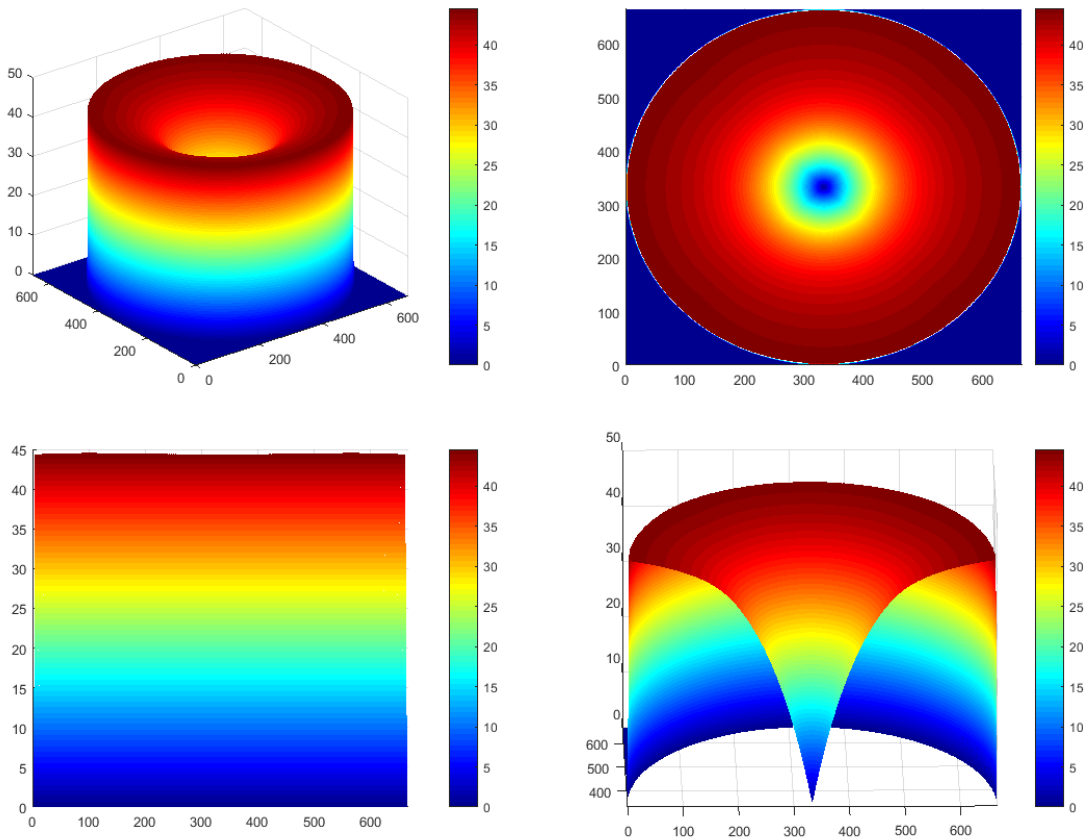

Fig. 9. Central section, range E = 0.6 ÷ 44.56 (V/m)

The distribution of the electric field strength occurs symmetrically from the center of the resonator, where E = 0.6 (V/m), to the edges, where the strength reaches E = 44.56 (V/m) (Figure 9).

The 2st step of the calculation is "Derivative 2".

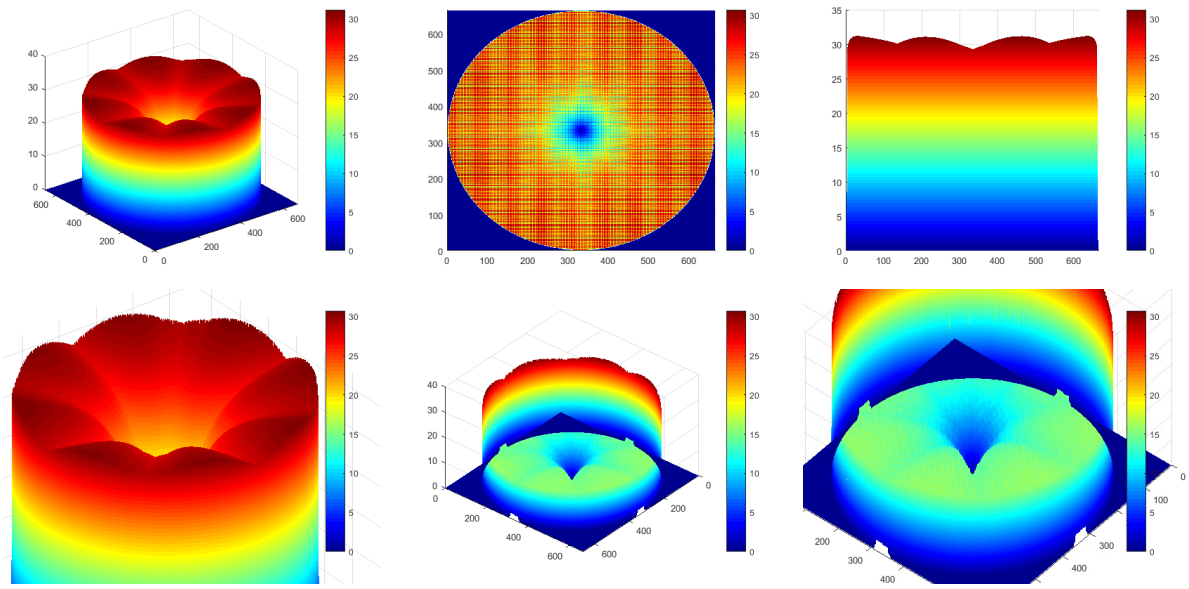

Fig. 10. Central section, range E = 0.6 ÷ 30.75 (V/m)

After the introduction of the three additional coordinate systems, arranged relatively orthogonal at 45°, there was a refinement of both the distribution diagram and the field strength parameters E = 32.75 (V/m) relative to the initial matrix obtained in the 1st stage of the calculation (Fig. 10).

The 3st step of the calculation is "Derivative 3".

The calculations of the third stage obtained a distribution of strength E and intensity I of the electromagnetic field in three-dimensional space (Fig. 11, 12).

In the central zone, we see:

- maximum strength followed by a sharp decrease over the circuit's center point: E = 13.34 ÷ 0.6 (V/m) (Figure 11);
- maximum intensity followed by a sharp decrease over the circuit's center point: I = 178.0 ÷ 0.37 (V/m^2) (Figure 12).

Thus, one can clearly see the electromagnetic field's characteristics' pronounced tendency to a minimum amplitude over the center of the circuit.

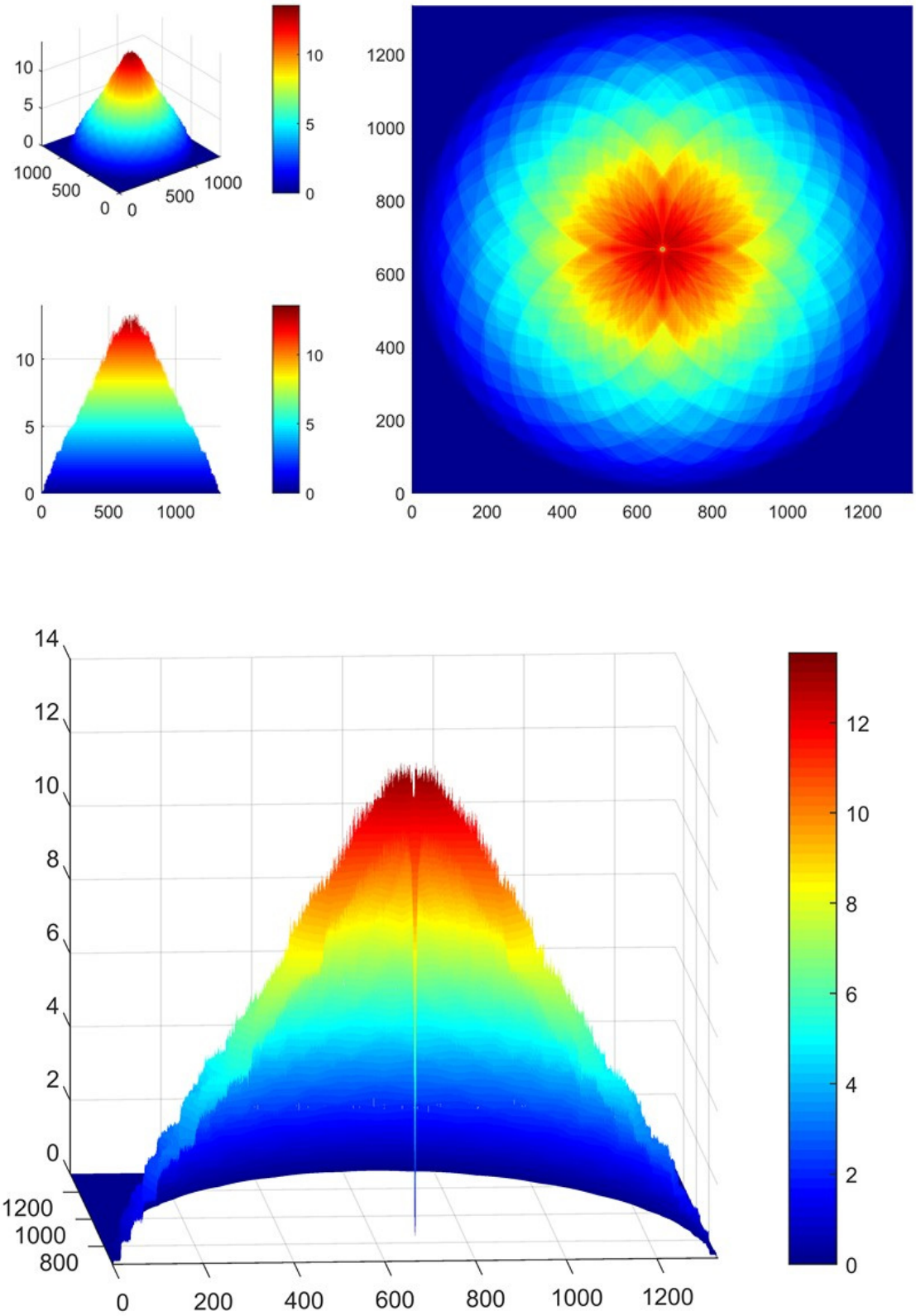

Fig. 11. Central section. Distribution of strength E (V/m) in different projections

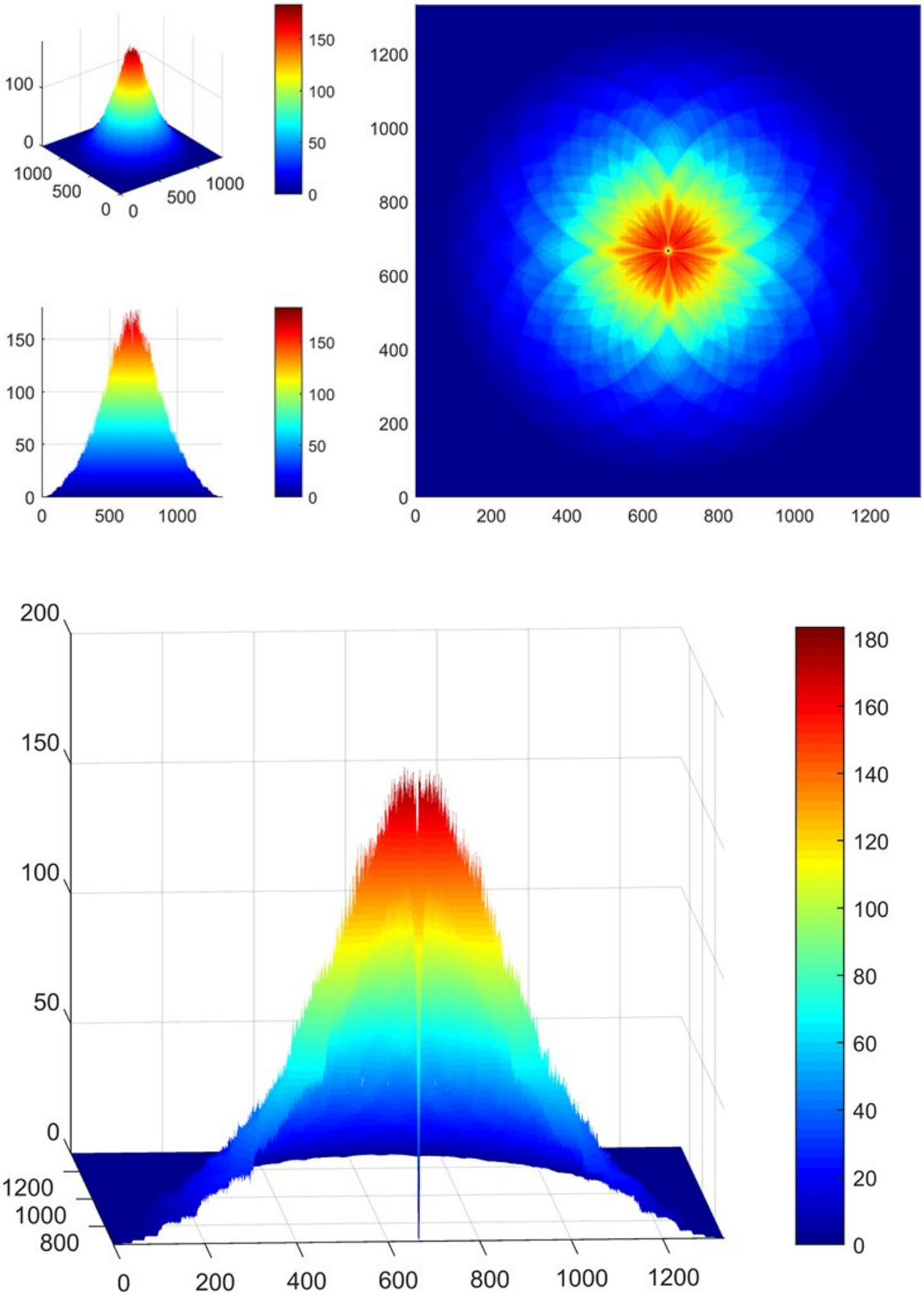

Fig. 12. Central section. Distribution of intensity I (V/m^2) in different projections

Figures 13-45 show the distribution of strength *E* and intensity *I* arising from the resonator of the field reflex with a height of 14.96 mm in various

horizontal sections with a step of 20*h* (0.45 mm) from the surface of the resonator.

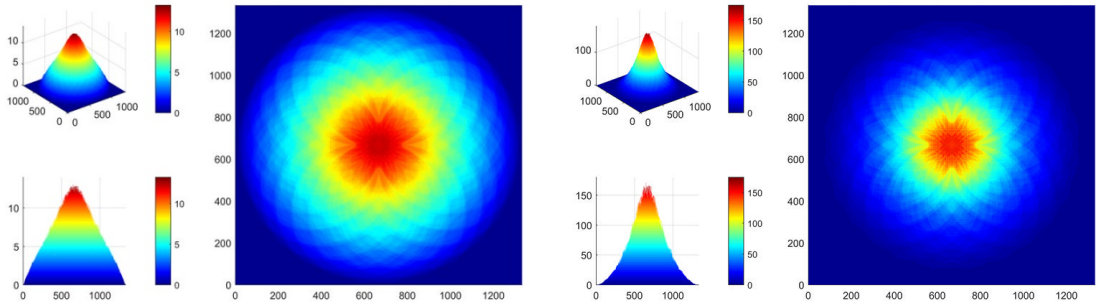

Fig.13. Strength (on the left) and intensity (on the right) at level 20 (0.45 mm)

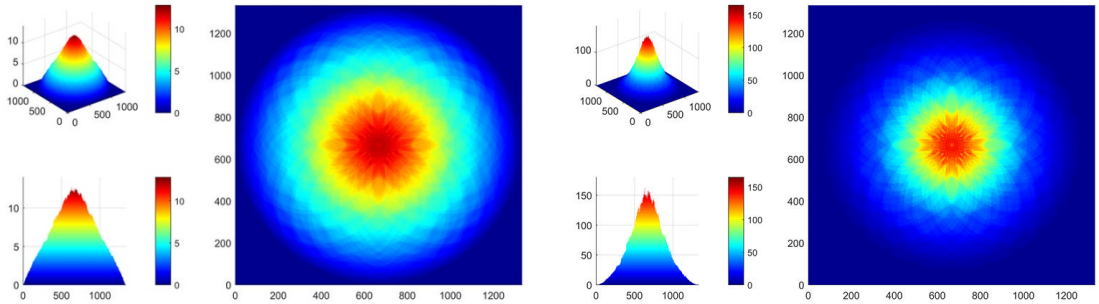

Fig.14. Strength (on the left) and intensity (on the right) at level 40 (0.9 mm)

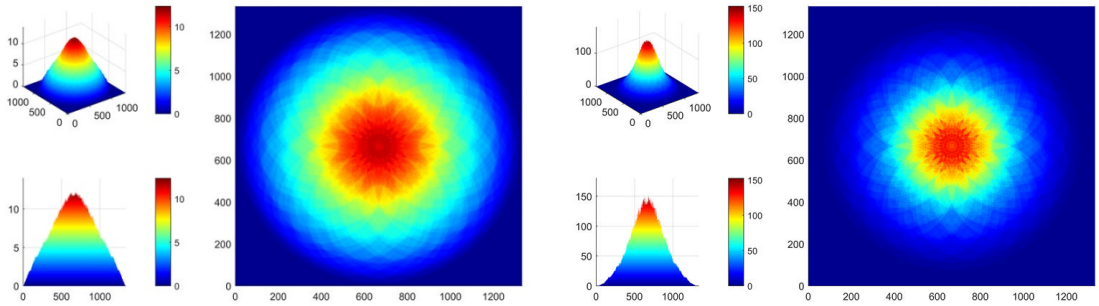

Fig.15. Strength (on the left) and intensity (on the right) at level 60 (1.35 mm)

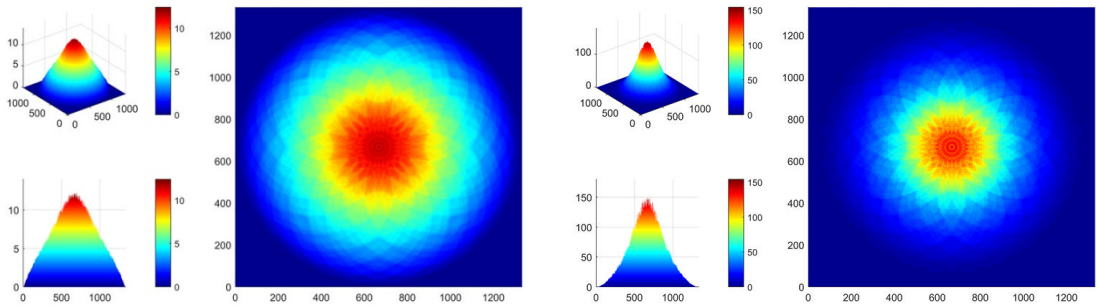

Fig.16. Strength (on the left) and intensity (on the right) at level 80 (1.8 mm)

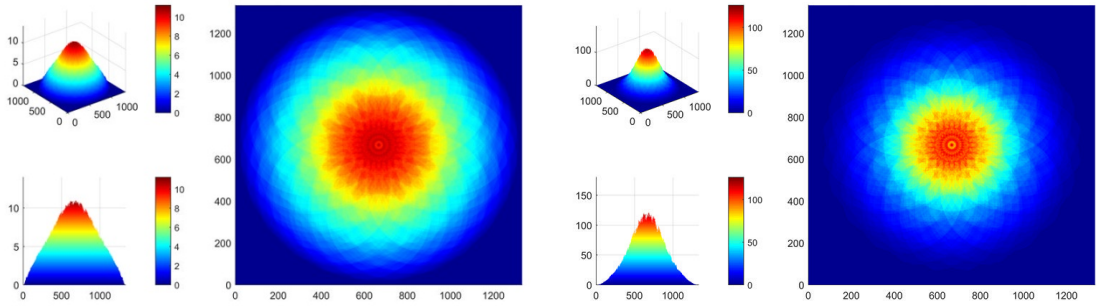

Fig.17. Strength (on the left) and intensity (on the right) at level 100 (2.25 mm)

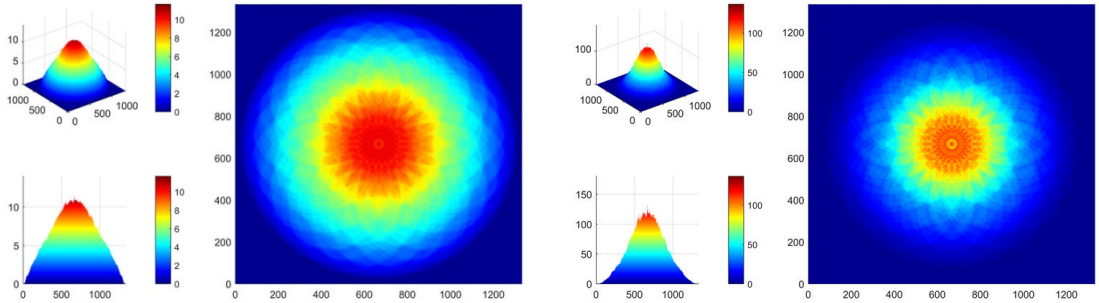

Fig.18. Strength (on the left) and intensity (on the right) at level 120 (2.7 mm)

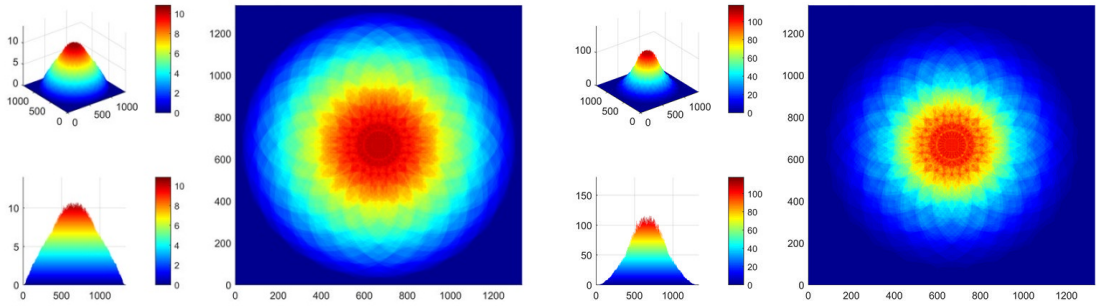

Fig.19. Strength (on the left) and intensity (on the right) at level 140 (3.15 mm)

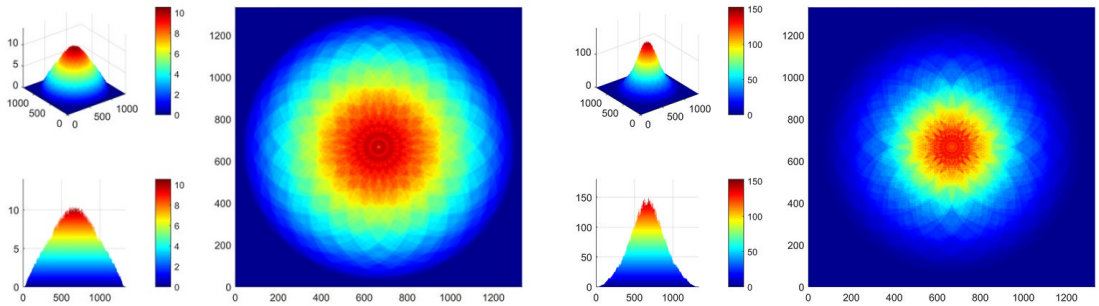

Fig.20. Strength (on the left) and intensity (on the right) at level 160 (3.6 mm)

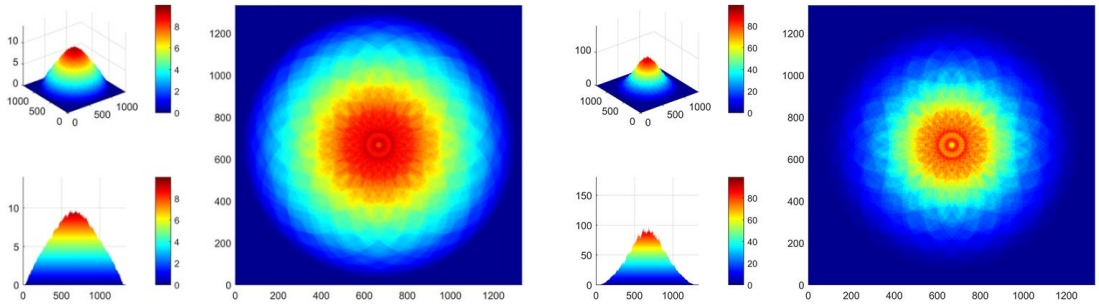

Fig.21. Strength (on the left) and intensity (on the right) at level 180 (4.05 mm)

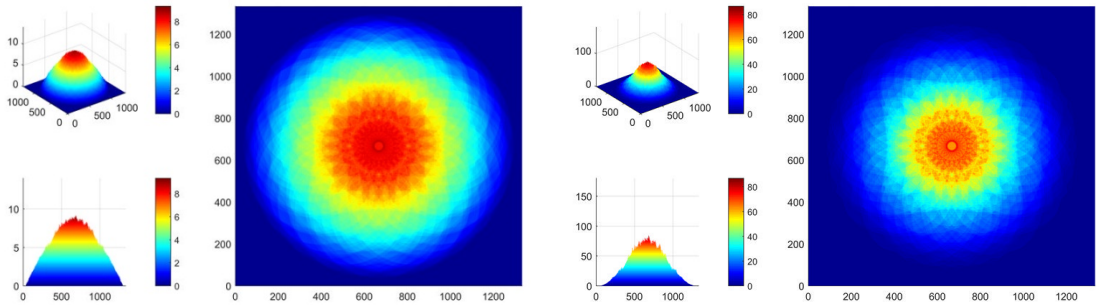

Fig.22. Strength (on the left) and intensity (on the right) at level 200 (4.5 mm)

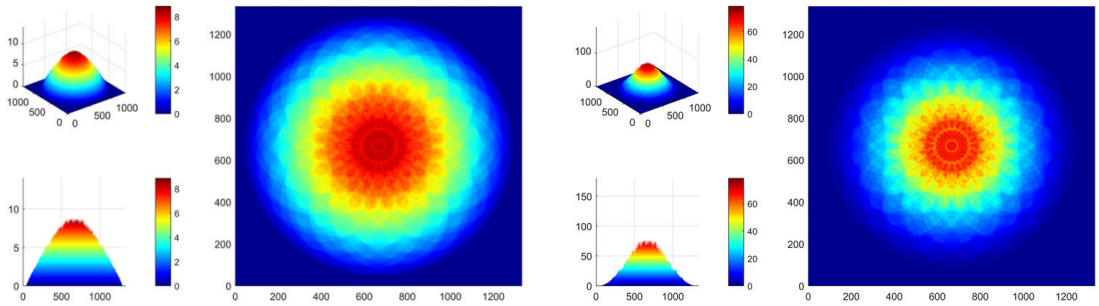

Fig.23. Strength (on the left) and intensity (on the right) at level 220 (4.95 mm)

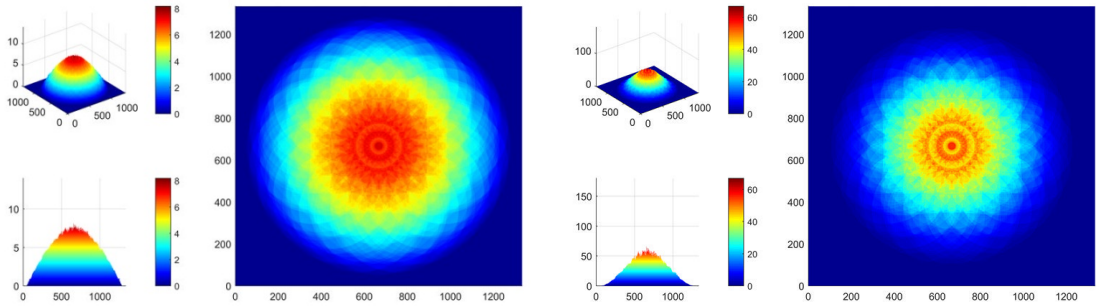

Fig.24. Strength (on the left) and intensity (on the right) at level 240 (5.4 mm)

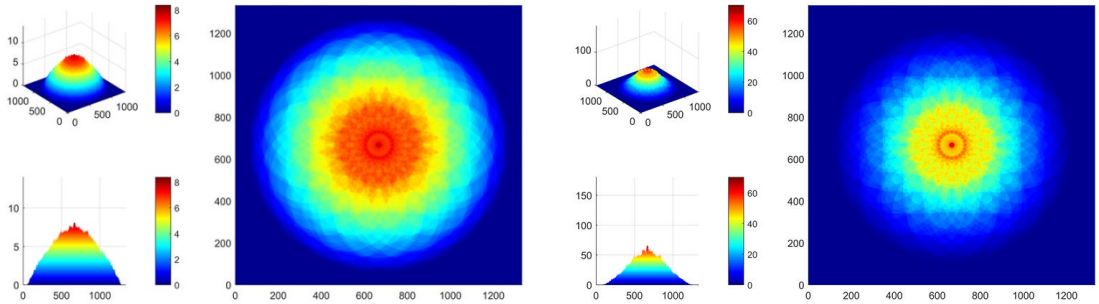

Fig.25. Strength (on the left) and intensity (on the right) at level 260 (5.85 mm)

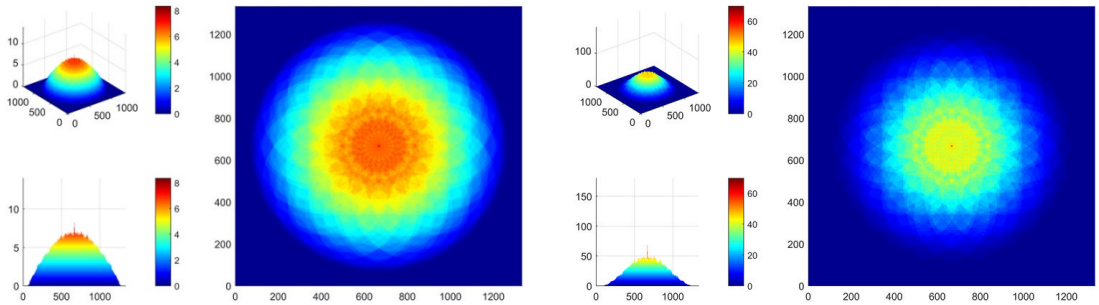

Fig.26. Strength (on the left) and intensity (on the right) at level 280 (6.3 mm)

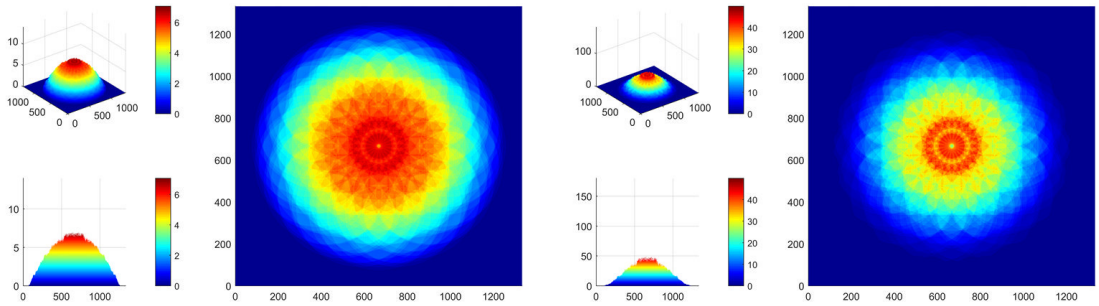

Fig.27. Strength (on the left) and intensity (on the right) at level 300 (6.75 mm)

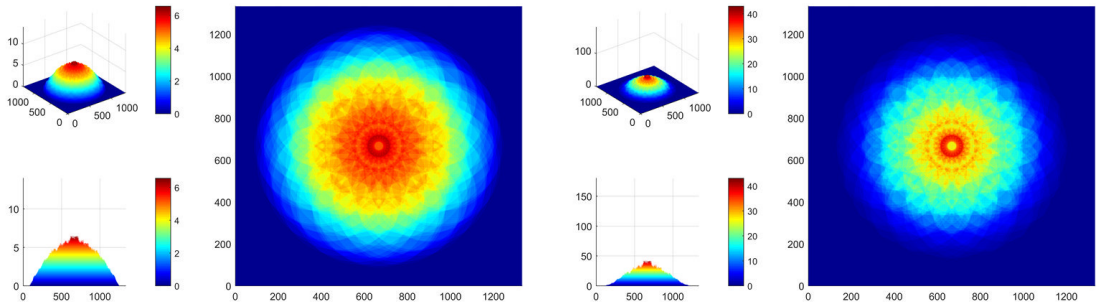

Fig.28. Strength (on the left) and intensity (on the right) at level 320 (7.2 mm)

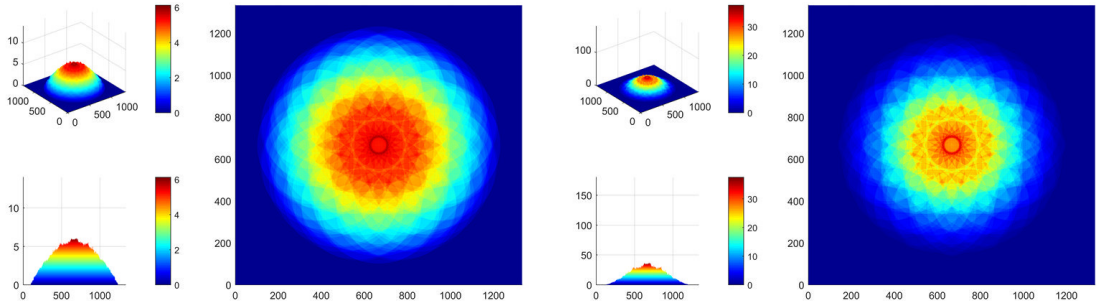

Fig.29. Strength (on the left) and intensity (on the right) at level 340 (7.65 mm)

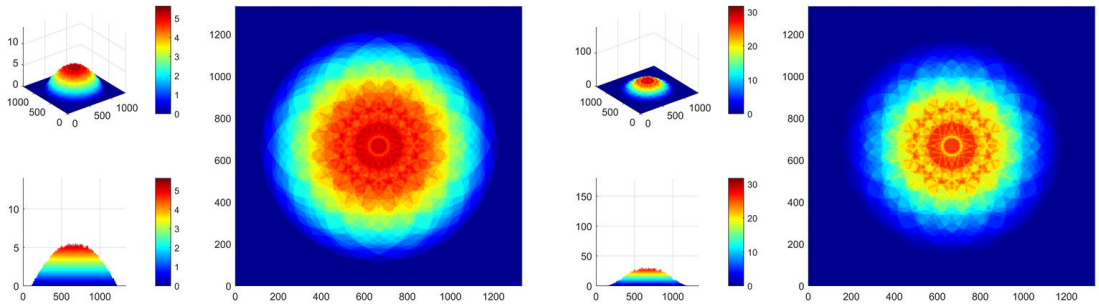

Fig.30. Strength (on the left) and intensity (on the right) at level 360 (8.1 mm)

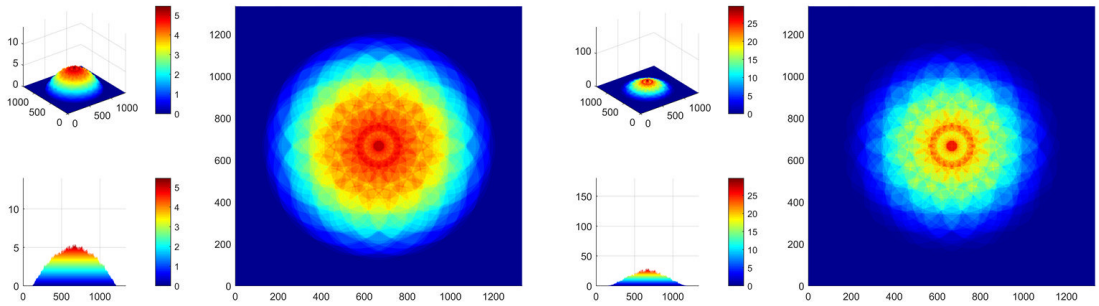

Fig.31. Strength (on the left) and intensity (on the right) at level 380 (8.55 mm)

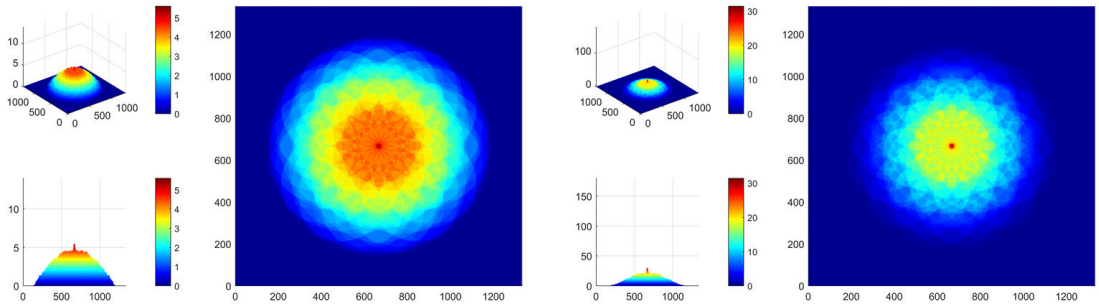

Fig.32. Strength (on the left) and intensity (on the right) at level 400 (9 mm)

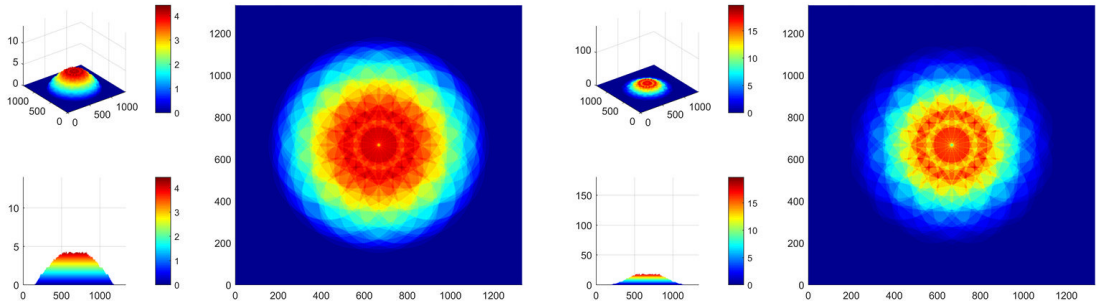

Fig.33. Strength (on the left) and intensity (on the right) at level 420 (9.45 mm)

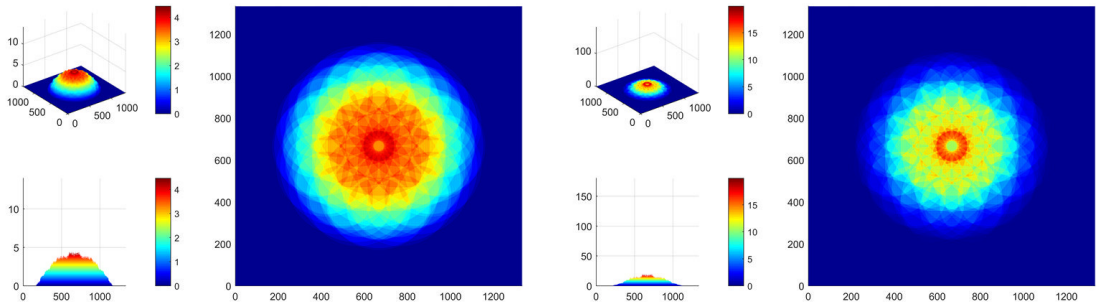

Fig.34. Strength (on the left) and intensity (on the right) at level 440 (9.9 mm)

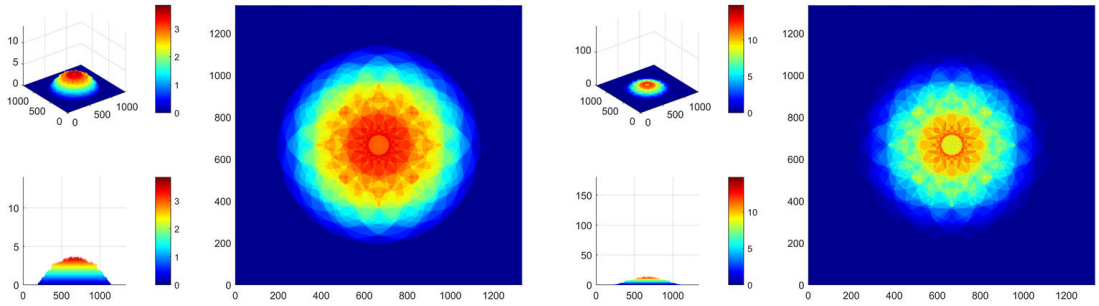

Fig.35. Strength (on the left) and intensity (on the right) at level 460 (10.35 mm)

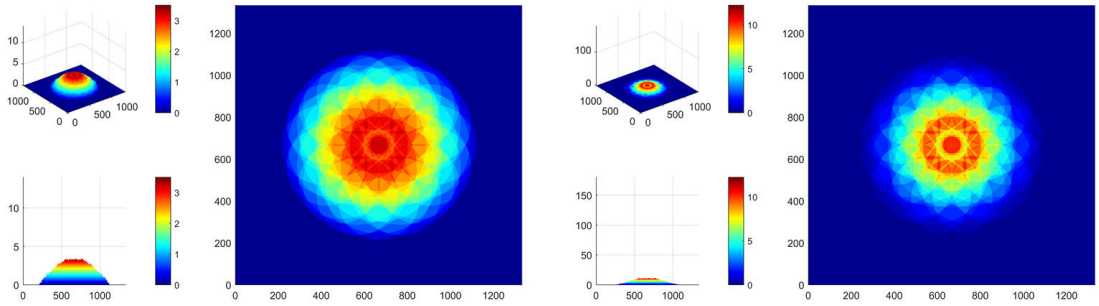

Fig.36. Strength (on the left) and intensity (on the right) at level 480 (10.8 mm)

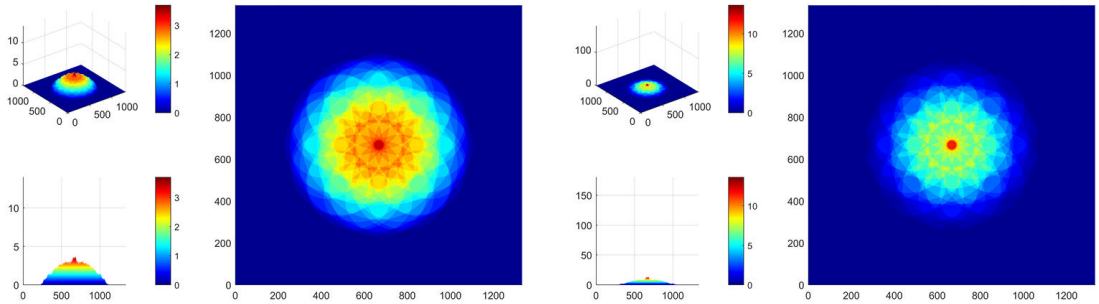

Fig.37. Strength (on the left) and intensity (on the right) at level 500 (11.25 mm)

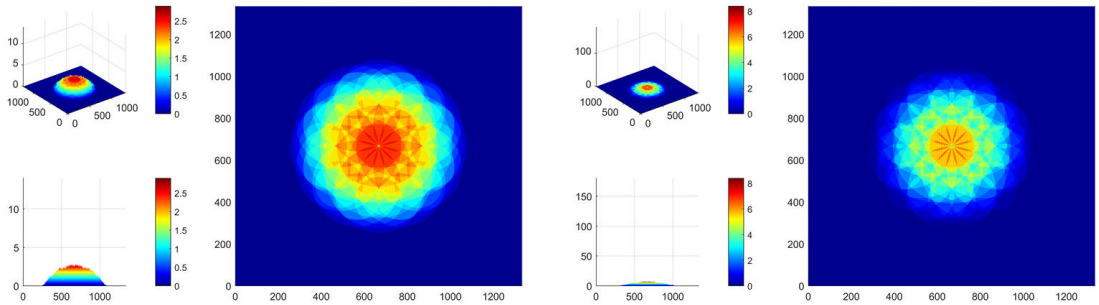

Fig.38. Strength (on the left) and intensity (on the right) at level 520 (11.7 mm)

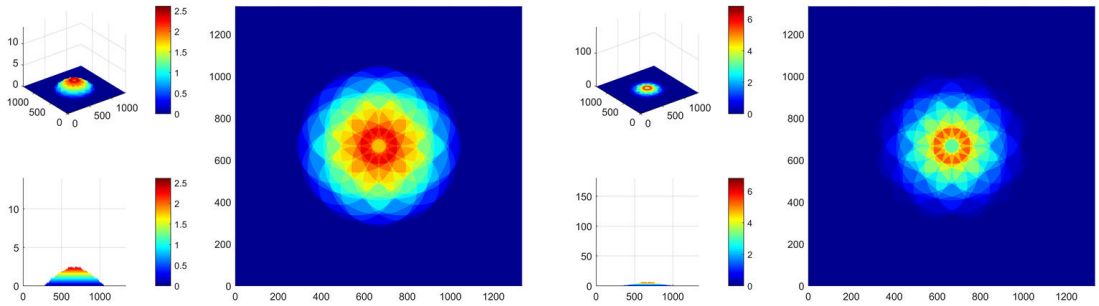

Fig.39. Strength (on the left) and intensity (on the right) at level 540 (12.15 mm)

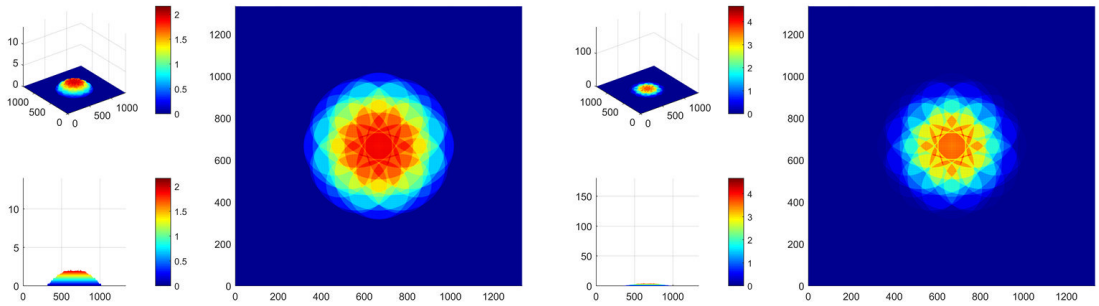

Fig.40. Strength (on the left) and intensity (on the right) at level 560 (12.6 mm)

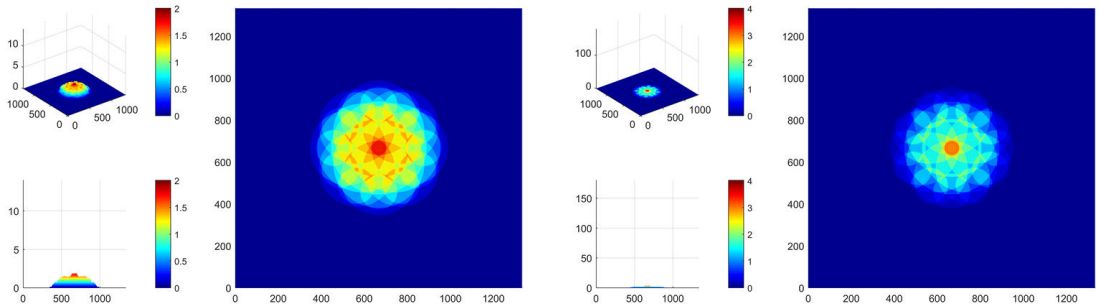

Fig.41. Strength (on the left) and intensity (on the right) at level 580 (13.05 mm)

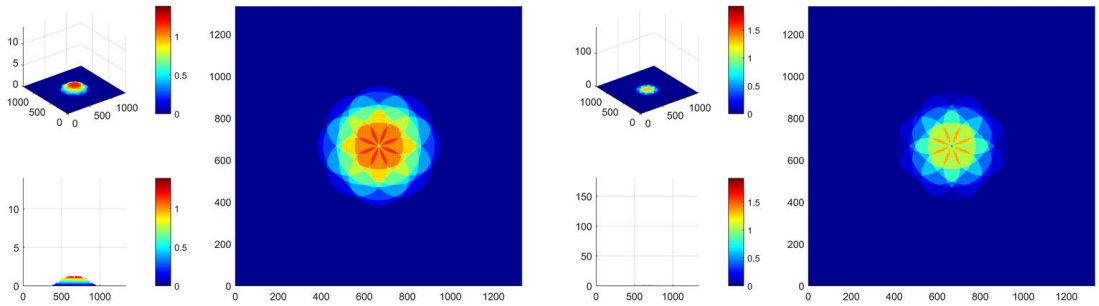

Fig.42. Strength (on the left) and intensity (on the right) at level 600 (13.5 mm)

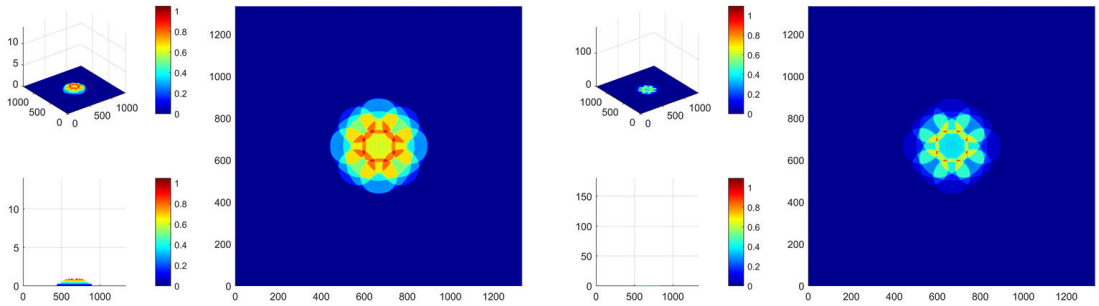

Fig.43. Strength (on the left) and intensity (on the right) at level 620 (13.95 mm)

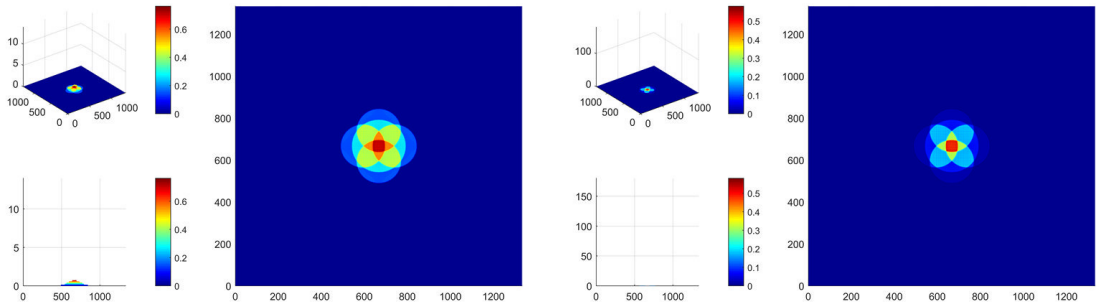

Fig.44. Strength (on the left) and intensity (on the right) at level 640 (14.4 mm)

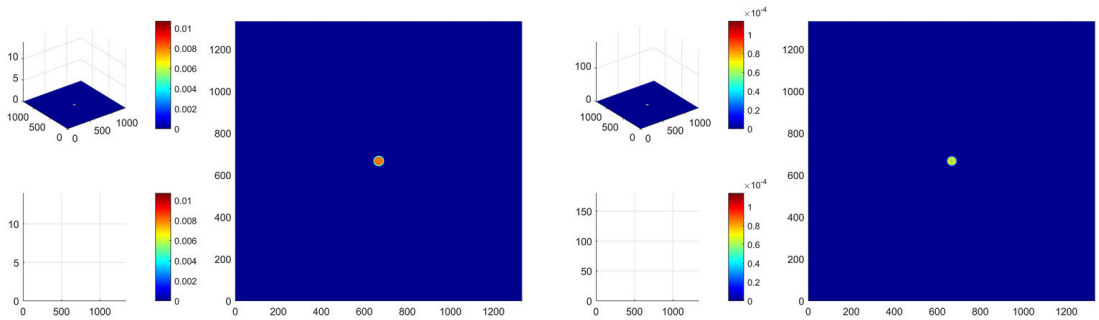

Fig.45. Strength (on the left) and intensity (on the right) at level 665 (14.96 mm)

As can be seen from Fig. 11, 12, when approaching the center of the circuit, the strength *E* increases, reaching its maximum values in the immediate vicinity of the center, as well as the energy flux density *I*. And in the very center, as a result of the counteraction of potentials of the ring of strength, when their values are multiplied, there is a sharp change in the characteristics of the electromagnetic field: the strength tends to a maximum, and the amplitude approaches zero. Thus, the circuit's central zone is analogous to the point of singularity in quantum physics, i.e. the energy density there is as high as possible, and the amplitude tends to zero, which corresponds to the previously presented the matching principle expressed by the formula (1), which also implies the formation of a resonant field analogous to the intrinsic topology of the resonator.

The consequence of this response is the redistribution of the field's energy flux density *I* with its nonlinear growth from the edges to the center of the resonator with a difference of ~ 481 times: from 0.37 $(V/m)^2$) to 178.0 (V/m^2). Further, within the ring of maximum response intensity, a counter resonance forms along its diameters, causing the values of the potentials participating in this process to be multiplied. As a result of counter-harmonization with respect to amplitudes, frequencies, phases, and the radiation pattern, there is a maximally neutral zone in the center and, since an active potential always redistributes from zones of maximum amplitude activity to a neutral zone, the potential density at the central point increases sharply and is constantly maintained, forming a stationary field, and the amplitude tends to zero, which initiates the singularity phenomenon (Fig 12). As a result, the focal point of the vector interaction of all processes with a common potential $(I_{max})^2 = (178.0)^2 = 31\ 684$ (V/m^2) emerges at the center.

Since the energy flux density of the field is proportional to the fourth power of the frequency: $I \sim \omega^4$, then the response frequency will also change:

$\Delta\omega \sim \sqrt[4]{\Delta I} = \sqrt[4]{481} = 4.68$, i.e. in 4.68 times will increase with respect to the original 2.4 GHz parameter and will be 11.23 GHz.

Thus, the directional harmonization of the wave processes with respect to amplitudes, phases, frequency, and the interaction diagram of the resonator's annular fractal topology initiates a stationary, maximally coherent point structure of high density with a minimum electric field intensity, which indicates the high neutrality of this zone.

In this case, the redistribution is not smooth and monotonic, but occurs in accordance with the profile features of the resonator's topological structure. Due to these features, the shape of the emerging field (electromagnetic superposition) over the resonator takes the form of a complex spatial hologram consisting of a large number of regular interpenetrating spherical surfaces of sizes that are multiples of one another and determined by the fractal structure and the dimensions of the annular grooves on the surface of the resonator.

When calculating the C28S resonator's interaction with incident radiation at a frequency of 2.4 GHz, analysis of the electric field strength E above the central point of the circuit at a height of 22.5 microns was performed over time with various intervals Δt.

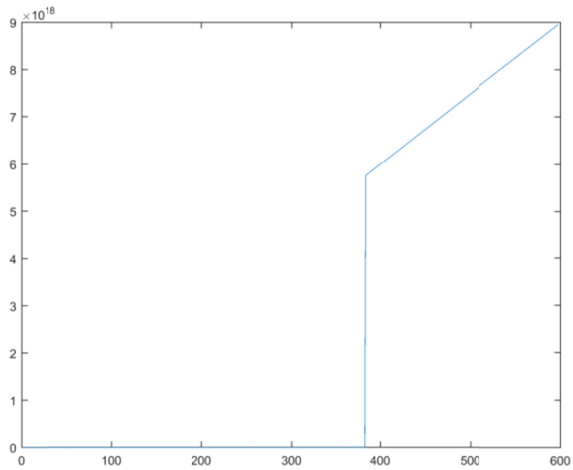

Fig. 46. $\Delta t = 10^7 s$, limit at $t = 383 * 10^7 s$

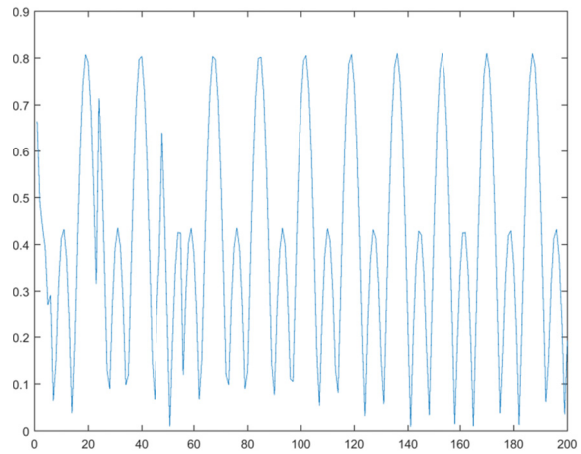

Fig. 47. $\Delta t = 10^7 s$, $\nu = 0.88$ Hz

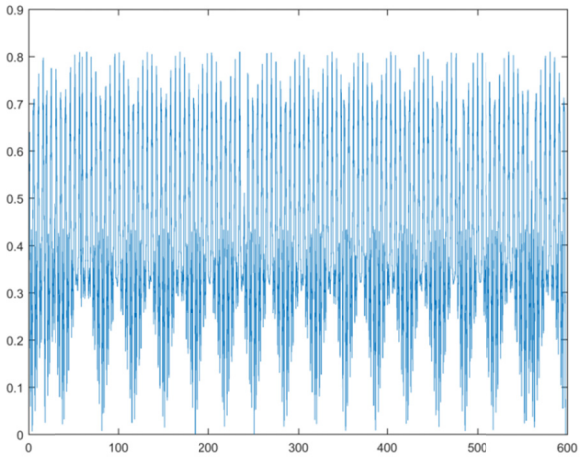

Fig. 48. $\Delta t = 10^6 s$, $\nu = 4.4$ Hz

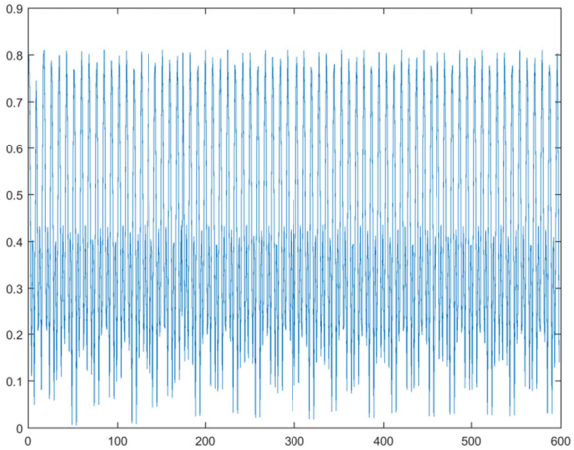

Fig. 49. $\Delta t = 10^5 s$

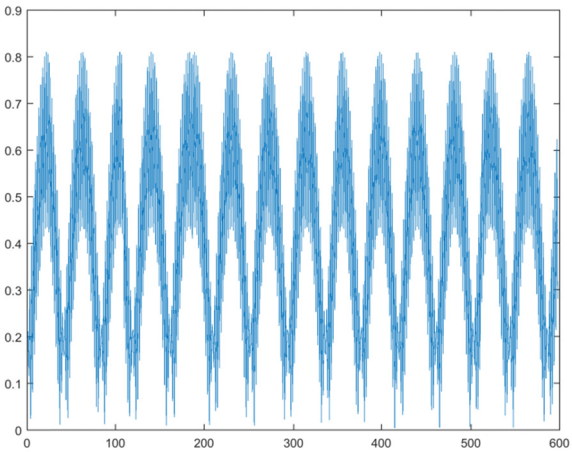

Fig. 50. $\Delta t = 10^4 s$, $\nu = 357$ Hz

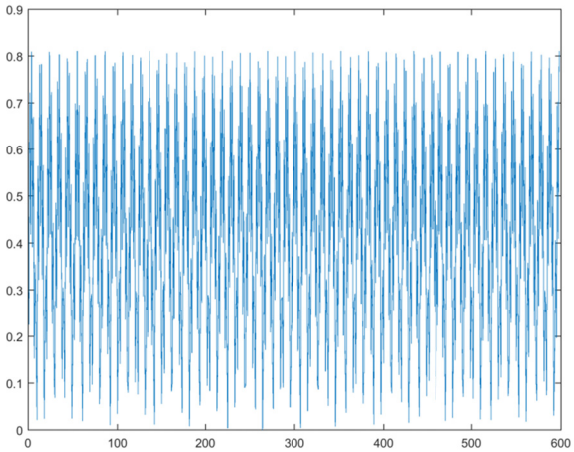

Fig. 51. $\Delta t = 10^3 s$

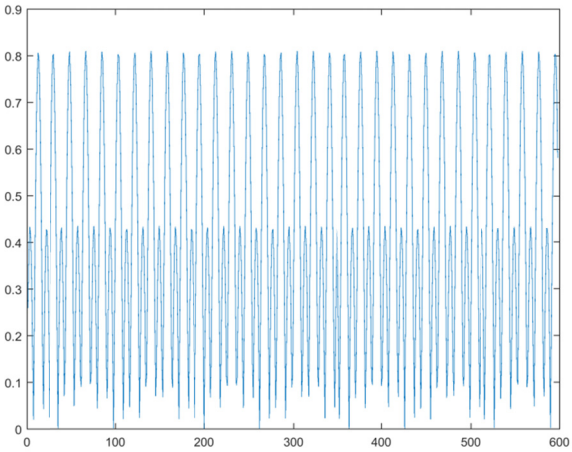

Fig. 52. $\Delta t = 100 s$, $\nu = 83.3$ kHz

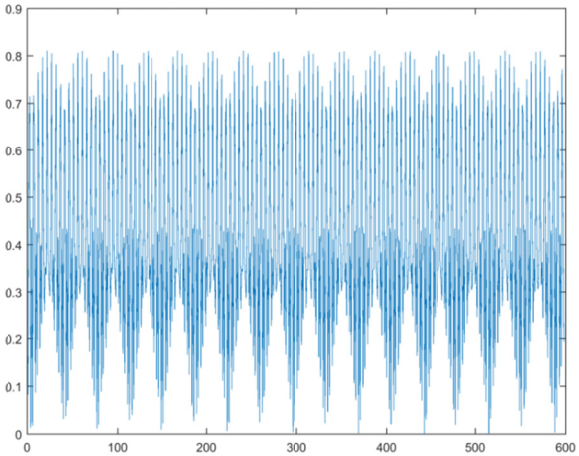

Fig. 53. $\Delta t = 10 s$, $\nu = 411$ kHz

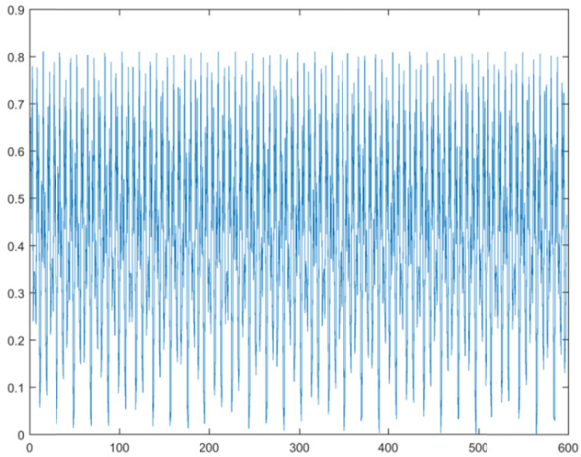

Fig. 54. Δt =1s

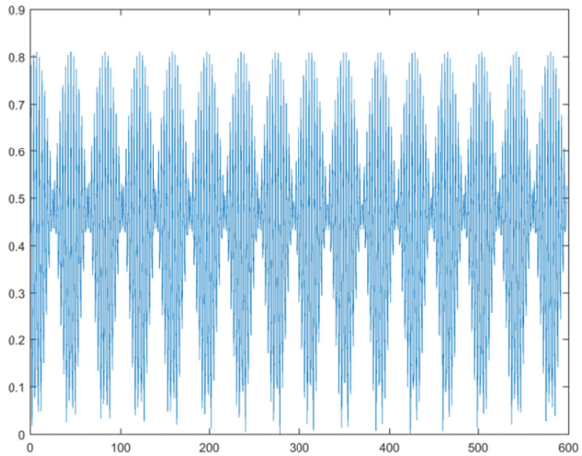

Fig. 55. Δt = 0.1s, ν = 41.7 MHz

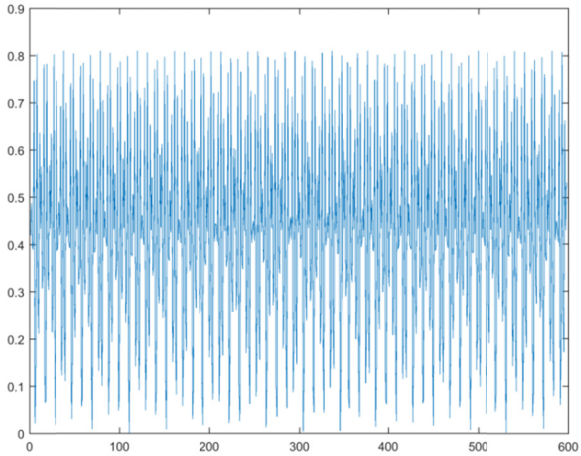

Fig. 56. Δt = 0.01s

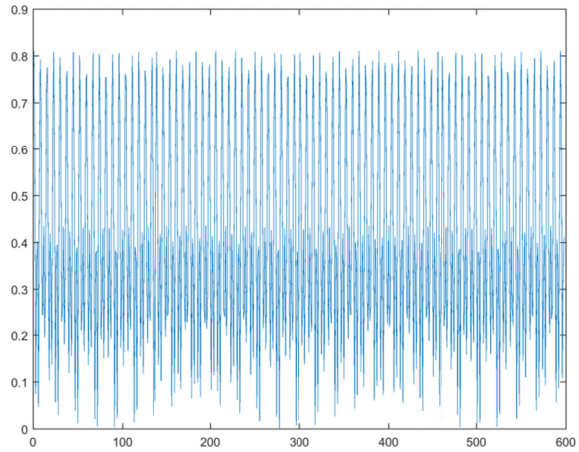

Fig. 57. Δt = 10^{-3}s

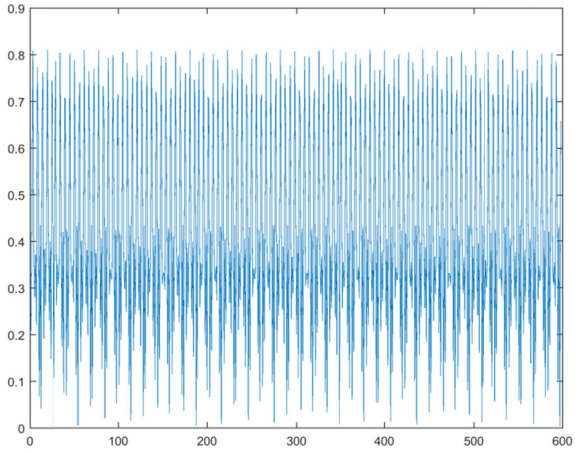

Fig. 58. Δt = 10^{-4}s

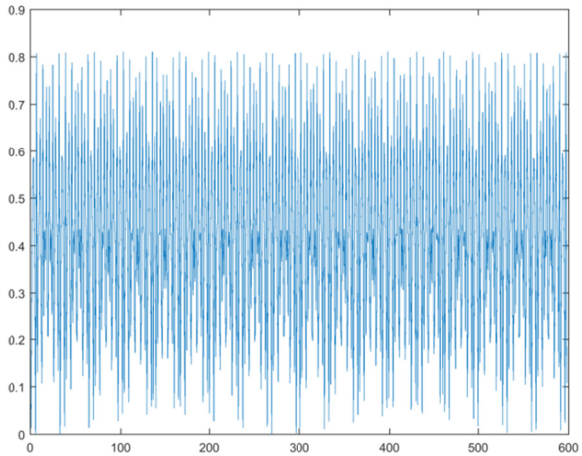

Fig. 59. Δt = 10^{-5}s

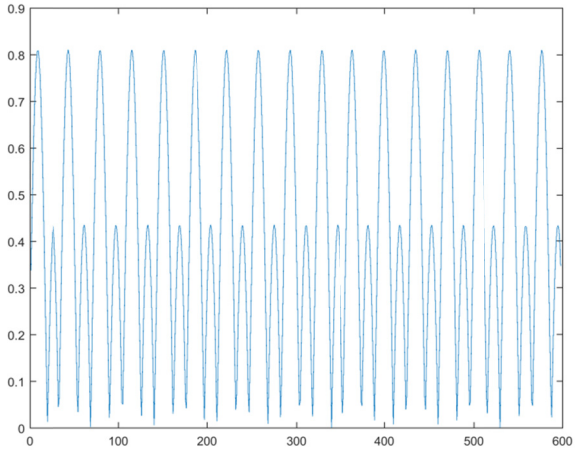

Fig. 60. $\Delta t = 10^{-6}s$, $\nu = 4.2$ THz

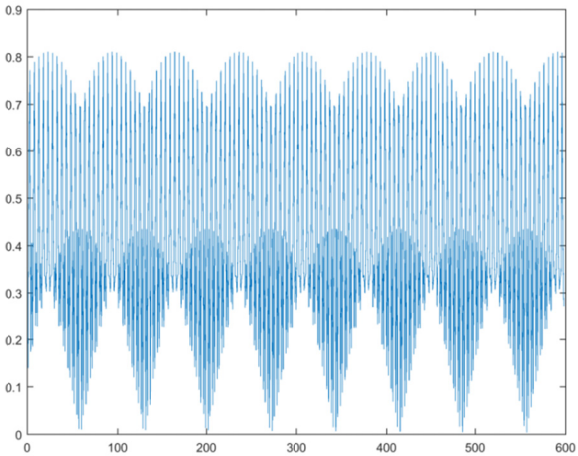

Fig. 61. $\Delta t = 10^{-7}s$

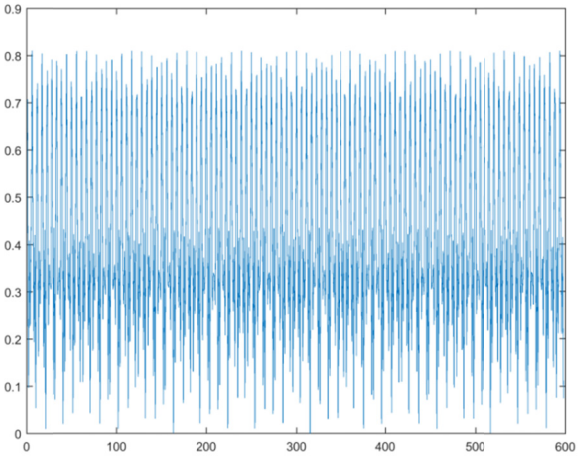

Fig. 62. $\Delta t = 10^{-8}s$

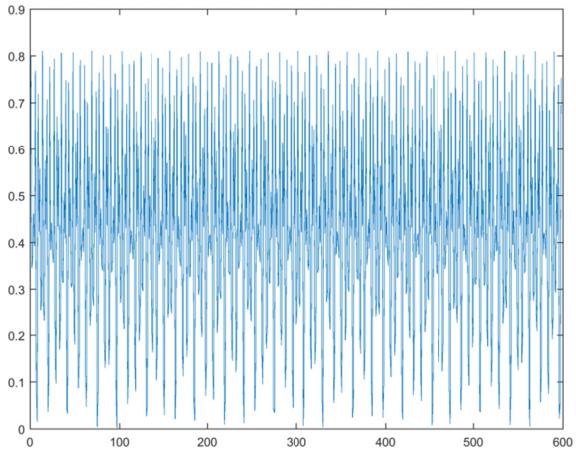

Fig. 63. $\Delta t = 10^{-9}s$

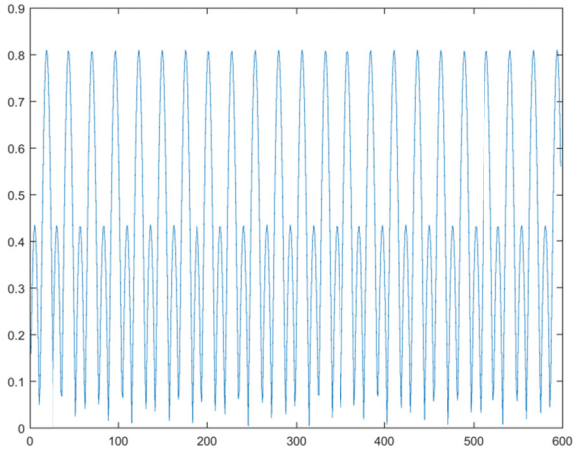

Fig. 64. $\Delta t = 10^{-10}s$, $\nu = 56.6$ PHz

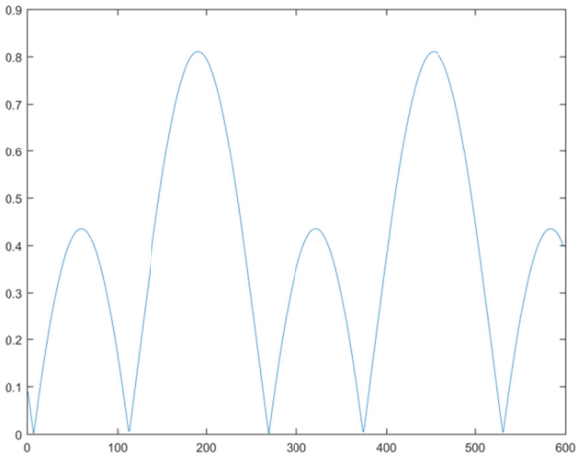

Fig. 65. $\Delta t = 10^{-11}s$

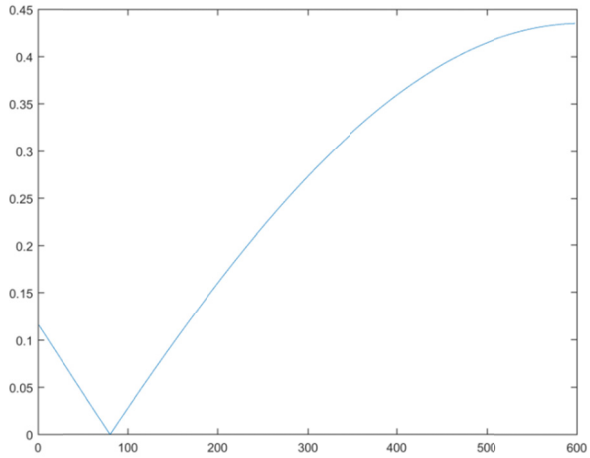

Fig. 66. $\Delta t = 10^{-12}s$

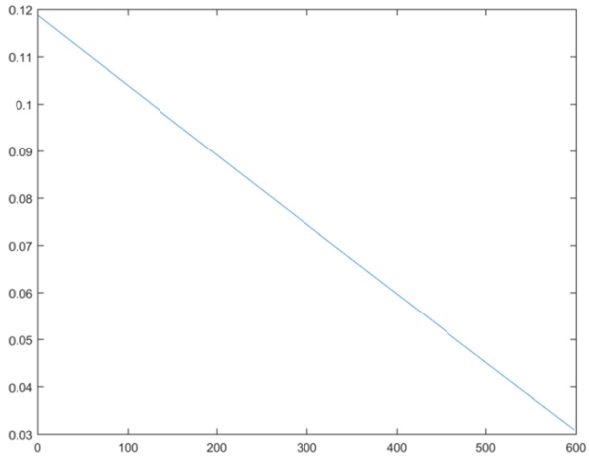

Fig. 67. $\Delta t = 10^{-13}s$

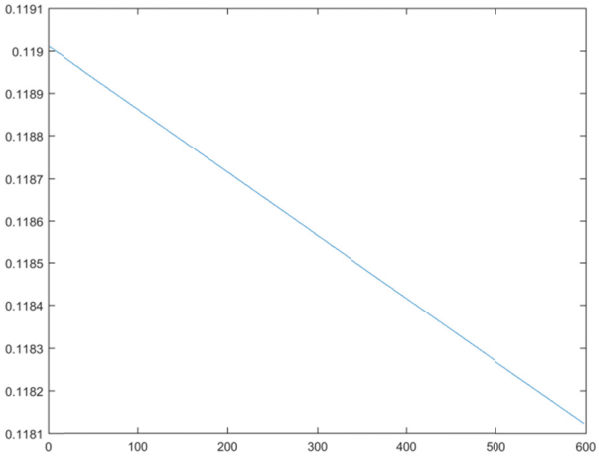

Fig. 68. $\Delta t = 10^{-15}s$

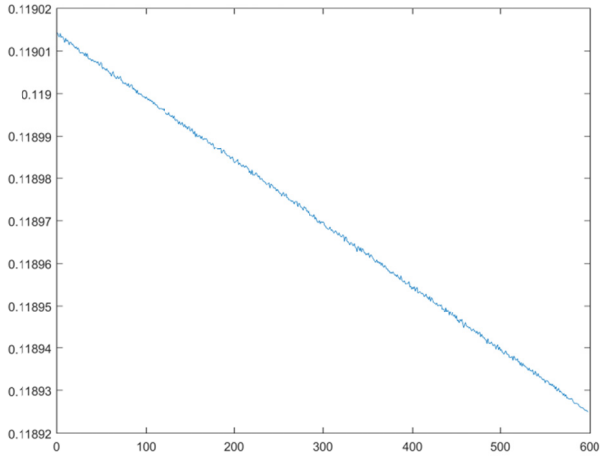

Fig. 69. $\Delta t = 10^{-16}s$

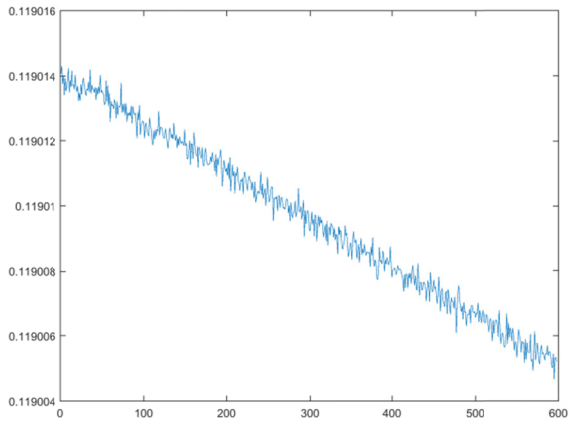

Fig. 70. $\Delta t = 10^{-17}s$

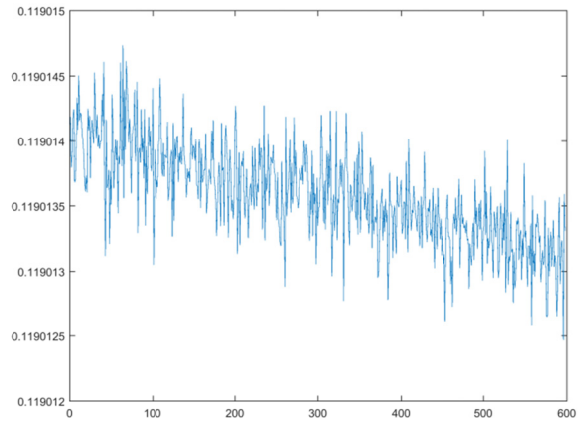

Fig. 71. $\Delta t = 10^{-18}s$

As can be seen from the presented images (Fig. 46-71), the regularity of the wave response has several levels in the time range: from 10^{7}s to 10^{-12}s. If the time step is reduced further, the pattern breaks down. Undoubtedly, this phenomenon associated with the system's discrete step requires additional studies. However, it can be noted that the superposition arising from the Aires

resonator (C28S) in the form of a stationary field response has a regular character on at least three levels of testing with the following frequencies:
ν_1 = 56.6 PHz (Figure 64); ν_2 = 4.2 THz (Figure 60); ν_3 = 83.3 kHz (Figure 52).

In summary, given external irradiation of the Aires microprocessor, the resonance response is an integral, stationary, highly coherent superposition from the interaction of surface waves with annular slits, concentrating the electric potential in them, thus causing them to begin working as waveguides. The points where the rings intersect initiate the phase matching of counter flows, thereby triggering the appearance of a stationary (standing) wave, which is clearly seen in the computer simulation. As a result, the emerging reflex represents a whole complex of corresponding, inter-integrated, fractal (self-similar) interactions.

The animation (Appendix 3) shows the consecutive responses of the Aires resonator (microprocessor) to the influence of electromagnetic radiation in different sections from the edge of the resonator to its center in the form of a distribution of the strength and energy flux density of the electromagnetic field.

CONCLUSION

The simulations showed that given electromagnetic action at a frequency of 2.4 GHz on an Aires self-affine resonator (microprocessor), the device converts incident electromagnetic radiation into a coherent spatio-temporal self-affine form (hologram). In particular, over the central region of the resonator, there is a marked increase in both the strength E_{max} = 13.34 (V/m) (~22.23 times) and the intensity of the electric field I_{max} = 178.0 (V/m^2) (~ 481 times).

Further, within the ring of maximum response intensity, a counter resonance forms along its diameters, causing the values of the potentials participating in this process to be multiplied. As a result of counter-harmonization with respect to amplitudes, frequencies, phases, and the radiation pattern, there is a maximally neutral zone in the center and, since an active potential always redistributes from zones of maximum amplitude activity to a neutral zone, the potential density at the central point increases sharply, and the amplitude tends to zero, which initiates the singularity phenomenon. According to the first law of thermodynamics (the law of conservation of energy), energy doesn't appear out of nowhere or vanish into nothing – rather it transforms from one state into another, which is what happens in the central point of the circuit as the point of singularity. As a result, the focal point of the vector interaction of all processes with a common potential arises at the center of the circuit:

$$(I_{max})^2 = (178.0)^2 = 31684 \text{ (V/m}^2\text{)}.$$

In addition, the constant inflow of potential from the outside, which strives to fill the circuit's neutral zone, ensures that the emerging superposition is highly stable.

Thus, the energy of radiation coming from a Wi-Fi source (router) and modern mobile communication equipment (smartphone, telephone, etc.), after interaction with the resonator, is redistributed in space and across frequencies, phases, and the interaction diagram, transforming into a self-affine stationary structure (hologram) corresponding to the self-affine topological lattice of a resonator carrying analogous properties (coherent transformation).

The field (electromagnetic superposition) (Fig. 72) that results from the AIRES resonator's (microprocessor's) interaction with incident radiation (2.4 GHz) is self-affine, possess traits of holograms, and, according to the Gabor-Denisyuk theory of holograms, which states that any hologram bears all the same traits as the agent initiating the hologram, becomes a coherent transformer of any waves that interact with it in the corresponding frequency range.

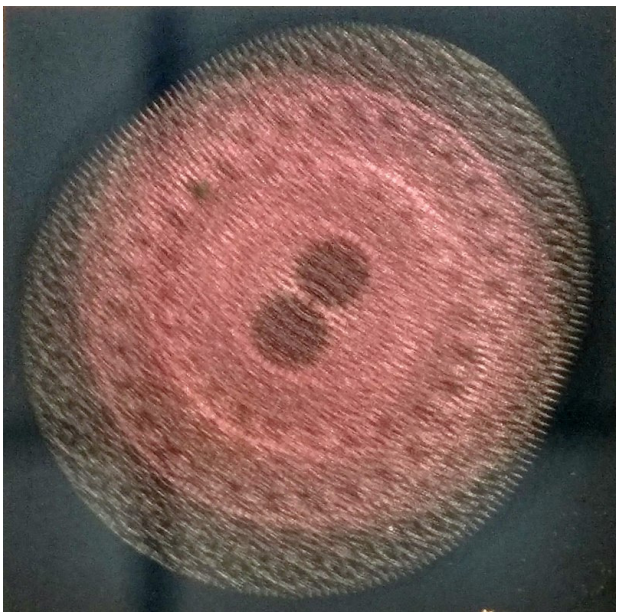

Fig. 72. Natural photograph of a hologram on the AIRES C28S microprocessor.

The results of the simulation demonstrate the redistribution of the characteristics of the electromagnetic field (strength and energy flux density), which reach their maximum values in the central part of the circuit, with a sharp condensation of the matched potential at its central point, which makes it possible to speak of the resulting stationary, spatial-wave electromagnetic reflex's ability to direct transform into a highly coherent form the electromagnetic radiation that interacts with it if that potential does not exceed the potential of the emerging reflex.

Based on the foregoing, we can state that the AIRES C28S microprocessor used in the Aires Defender Pro (2018 model) is a space-time amplitude-frequency converter (Fourier filter) that converts a dynamic wave pattern (2.4 GHz) into a stationary electromagnetic field that harmonizes external incident radiation in terms of amplitudes, frequencies, phases and the interaction diagrams and, thus, is a catalyst for coherent transformation of electromagnetic radiation interacting with it in the corresponding range of amplitudes and frequencies.

Consequently, in the presence of this resonator (AIRES microprocessor), the effect of harmonizing the external man-made radiation (2.4 GHz) with a biological organism's inherent radiation will be clearly expressed, which is confirmed by numerous tests with living objects, including the human body.

A comparative analysis of the results of modeling the interaction of electromagnetic radiation at 2.4 GHz (WiFi) with Aires resonators (microprocessors) with topological schemes C16S and C28S revealed the

following limiting values of the electromagnetic field strength *E* and the intensity *I*:

Table 2

Aires C16S	Min Value	Max Value	Increase (multiple)
E, V/m	1.3	12.73	9.79
I, V/m^2	1.76	162.2	92.16

Table 3

Aires C28S	Min Value	Max Value	Increase (multiple)
E, V/m	0.6	13.34	22.23
I, V/m^2	0.37	178.0	481

As can be seen from Tables 2, 3 when the circuit density changes from 16 to 28 fractalization axes (Aires C16S - Aires C28S), the range of the limit values of the strength E and the intensity I of the electromagnetic field increases and its degree is: for the intensity E – in 2.27 times (22.23/9.79=2.27) and intensity I – in 5.22 times (481/92.16=5.22) respectively.

Due to the fact that, according to Noether's theorem (2), a system with higher-level symmetry, due to the different discrete step that determines the system's density, is more stable, and the emerging wave superposition has properties analogous to the substrate, which determines a higher selectivity of interactions with external radiation. As a result, based on our calculations, we can say that relative to the Aires C16S the efficiency of the Aires C28S microprocessor increases in proportion to the degree of increase in the intensity range, i.e. ~ 5.22 times.

Thus, the transition to a denser topology (C16S – 83521, and C28S - 707281 ring resonators) is justified, since the Aires C28S microprocessor used in the Aires Defender Pro (2018 model) is more efficient (~ 5.22 times) than the Aires C16S microprocessor used in the Aires Shield Pro (2018 model).

Appendix 1

TOPOLOGY OF THE AIRES C28S RESONATOR (MICROPROCESSOR)

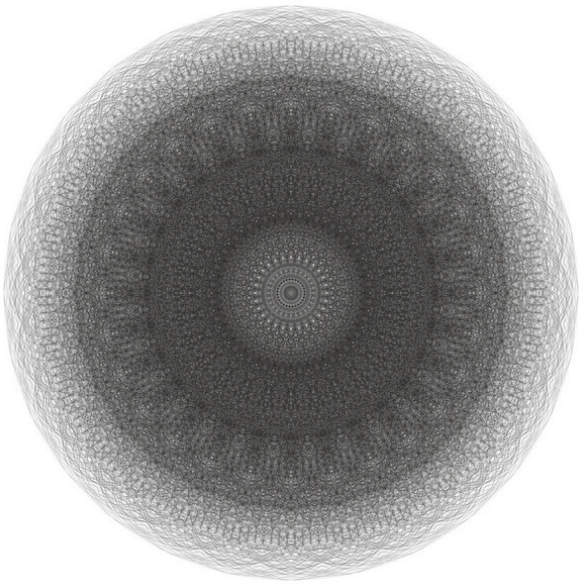

Appendix 2

HARDWARE AND SOFTWARE

Hardware:

- Server: Supermicro CSE-733TQ-665B
- Processor: Intel Xeon E5-2620 v2 2.1 GHz (6-core) x 2.
- RAM: Kingston DDR3-1600 MHz, 96 GB
- Video card: ASUS GeForce GT 740

Software:

- PascalABC.NET v.3.3
- MATHLAB R2015b

Appendix 3

ANIMATION

The dynamics of the computer simulation process can be viewed here: https://yadi.sk/i/OFuT7q8X3XTcvR.